Available online at www.sciencedirect.com
SCIENCE DIRECT®
Journal of Computational Physics 194 (2004) 544–574
JOURNAL OF COMPUTATIONAL PHYSICS
www.elsevier.com/locate/jcp

Studies of the accuracy of time integration methods for reaction–diffusion equations ☆

David L. Ropp [a], John N. Shadid [b,*], Curtis C. Ober [c]

[a] *Department of Computational Mathematics and Algorithms, MS 1110, P.O. Box 5800, Sandia National Laboratories, Albuquerque, NM 87185-1110, USA*
[b] *Department of Computational Science, MS 1111, P.O. Box 5800, Sandia National Laboratories, Albuquerque, NM 87185-1111, USA*
[c] *Department of Computational Science, MS 0316, P.O. Box 5800, Sandia National Laboratories, Albuquerque, NM 87185-0316, USA*

Received 21 May 2003; received in revised form 15 August 2003; accepted 22 August 2003

Abstract

In this study we present numerical experiments of time integration methods applied to systems of reaction–diffusion equations. Our main interest is in evaluating the relative accuracy and asymptotic order of accuracy of the methods on problems which exhibit an approximate balance between the competing component time scales. Nearly balanced systems can produce a significant coupling of the physical mechanisms and introduce a slow dynamical time scale of interest. These problems provide a challenging test for this evaluation and tend to reveal subtle differences between the various methods. The methods we consider include first- and second-order semi-implicit, fully implicit, and operator-splitting techniques. The test problems include a prototype propagating nonlinear reaction–diffusion wave, a non-equilibrium radiation–diffusion system, a Brusselator chemical dynamics system and a blow-up example. In this evaluation we demonstrate a "split personality" for the operator-splitting methods that we consider. While operator-splitting methods often obtain very good accuracy, they can also manifest a serious degradation in accuracy due to stability problems.
© 2003 Elsevier Inc. All rights reserved.

1. Introduction

In this paper we consider the numerical solution of time dependent, nonlinear, partial differential equations (PDEs) of reaction–diffusion problems. These equations are a subset of more general systems of coupled, highly nonlinear PDEs that exhibit solutions with multiple time and length scales [2,3,11]. Specifically, we are interested in reaction–diffusion systems that exhibit multiple competing time scales that

☆ This work was partially supported by ASCI program and the DOE Office of Science MICS program at Sandia National Laboratory under Contract DE-AC04-94AL85000.
* Corresponding author. Tel.: +1-505-845-7876; fax: +1-505-845-7442.
E-mail addresses: dlropp@sandia.gov (D.L. Ropp), jnshadi@sandia.gov (J.N. Shadid), ccober@sandia.gov (C.C. Ober).

0021-9991/$ - see front matter © 2003 Elsevier Inc. All rights reserved.
doi:10.1016/j.jcp.2003.08.033

nearly balance, to produce a slower dynamical time scale. Recently, there has been considerable interest in evaluating accepted time integration techniques for these systems [11]. To date, the most comprehensive studies have been applied to the non-equilibrium radiation–diffusion equations [11–14,18].

The existence of multiple fast component time scales that interact, to produce a slower dynamical time scale, necessitates the use of some amount of implicitness in the time integration technique. Invariably these algorithms lead to large nonlinear and linear algebraic systems. For this reason the robust and accurate solution of these problems is very challenging. In practice, for these systems, time integration is most often carried out by using some type of low-order time-step expansion or operator-splitting techniques [2,3]. These techniques do not fully converge the nonlinearities of the system and attempt to reduce the cost and complexity of the transient solution at each time step. Inherent in a number of these methods is a failure to maintain, accurately, the approximate balance of the competing time scales. For example, low-order expansion techniques produce semi-implicit schemes which can be solved in one step with a single linear solve and therefore by-pass the need for nonlinear solvers. Operator-splitting methods simplify the nonlinear system by separating the physics operators in each equation (or system of equations) into individual equations. These individual equations are then time integrated with solvers tailored for the particular characteristics of the physics operators. The combined effect of the split physics is then approximated by fractional-step methods [15,30], or a composition of sequential operators [19]. The advantage of these techniques is a reduction in the complexity of the component solves. For a given time-step size, all these methods clearly can exchange temporal accuracy and/or possibly numerical stability for computational efficiency.

In this context recent studies have been reported that compare the accuracy of linearized schemes and operator-splitting schemes, with fully implicit schemes that converge the nonlinearity of the solution at each time step [12–14,18]. These studies show that, in the absence of spatial discretization errors, the first-order linearization schemes exhibit a significant degradation of accuracy relative to the fully implicit methods. In [14,18], it is further demonstrated that second-order linearization techniques can be used, with consideration of both space and time discretization errors, to produce techniques that exhibit similar error bounds as a fully converged fully implicit method. Further, results in [18] show that, depending on the problem, operator-splitting methods can be more or less accurate than fully implicit methods. Our new results verify and extend these results as well.

Our work also extends this current literature by comparing linearized, fully implicit, and operator-splitting methods, each at first- or second-order, on a number of new test problems. In this study, we have investigated several aspects of the approximations to four nonlinear reaction–diffusion PDEs. The first test problem is a thermal wave [10] which has a smooth analytic solution with a propagating front. This front is maintained by a balance between the diffusion and reaction operators. The thermal wave problem has a constant diffusion coefficient and therefore produces a linear component solve for the diffusion operator in an operator-splitting method. Additional details of the thermal wave problem are given in Section 5.1.

The second test problem is the Brusselator problem [20]. These equations, originally studied as a model for chemical dynamics, exhibit a wide range of behavior. In our numerical experiments we confine the parameter range of interest to produce oscillatory solutions. As with the thermal wave problem, the diffusion coefficient is constant so that the component solve for the diffusion operator is linear. Additional details of the Brusselator problem are given in Section 5.2.

The third test problem is actually a set of two test sub-problems which model blow up [1,23]. Both have a quadratic source term nonlinearity and will exhibit blow up in finite time for sufficiently large initial conditions. The first of these has a linear diffusion operator while the second has a nonlinear diffusion operator. Additional details of the blow-up problem are given in Section 5.3.

The fourth test problem is a non-equilibrium radiation–diffusion problem. This problem consists of two coupled equations for the radiation energy density and material temperature. This problem has a nonlinear diffusion operator in the radiation energy density equation. Further details on this problem can be found in the literature [12,13,28]. The details of the specific test problem are described in Section 5.4.

The remainder of the paper is structured as follows. In Section 2, we give a heuristic argument to demonstrate that a problem with two comparable time scales can have a completely different dynamic time scale. In Section 3, we present the Galerkin finite element method (FEM) formulation, in a generalized form, for reaction–diffusion equations. The time integration methods investigated in this study are then presented in Section 4. The specific implementation for each test problem is discussed in Section 5. In Section 6, we present the details related to the ODE solvers used in this study. And finally in Section 7, we present and discuss the results from the numerical experiments. We then present a number of conclusions in Section 8.

2. Heuristic comparison of time scales

When two processes with different time scales are coupled together, the resulting dynamic time scale can be very different from either of the original time scales. Although it is not the goal of this paper to determine the time scales of reaction–diffusion systems, in this section we use a heuristic example to demonstrate how such a disparity between time scales can occur.

We start with a general reaction–diffusion equation

$$\frac{\partial \chi}{\partial t} + \nabla \cdot \mathbf{j} - S(\chi) = 0,$$

where $\mathbf{j} = -D\nabla\chi$. In a manner similar to [11] we use a simple dimensional argument to define the time scales of the component operators. Then defining the characteristic time scales as the absolute value, we have

$$\frac{1}{\tau_{\text{dyn}}} = \left|\frac{1}{\chi}\frac{\partial \chi}{\partial t}\right|, \quad \frac{1}{\tau_{\text{D}}} = \left|\frac{1}{\chi}\nabla \cdot D\nabla\chi\right|, \quad \frac{1}{\tau_{\text{S}}} = \left|\frac{S}{\chi}\right|.$$

Here the reaction time scale is τ_{S}, the diffusion time scale is τ_{D}, and the resulting dynamical time scale is τ_{dyn}. From the governing equation, we have that

$$\left|\frac{1}{\tau_{\text{D}}} - \frac{1}{\tau_{\text{S}}}\right| \leqslant \frac{1}{\tau_{\text{dyn}}} \leqslant \frac{1}{\tau_{\text{D}}} + \frac{1}{\tau_{\text{S}}},$$

or

$$\frac{\tau_{\text{D}}\tau_{\text{S}}}{\tau_{\text{D}} + \tau_{\text{S}}} \leqslant \tau_{\text{dyn}} \leqslant \frac{\tau_{\text{D}}\tau_{\text{S}}}{|\tau_{\text{D}} - \tau_{\text{S}}|}.$$

Next we consider different cases. First, if the reaction time scale is much less than the diffusion time scale, we have

$$\tau_{\text{S}} \ll \tau_{\text{D}},$$

$$\tau_{\text{dyn}} \approx \tau_{\text{S}}.$$

Similarly, if the diffusion time scale is much less than the reaction time scale, we have

$$\tau_{\text{D}} \ll \tau_{\text{S}},$$

$$\tau_{\text{dyn}} \approx \tau_{\text{D}}.$$

Thus, if the diffusion and reaction time scales differ by an order of magnitude or more, we expect the smaller of the two to be the time scale of the overall dynamics. Finally, we consider the case when τ_{D} and τ_{S} are comparable. Assume that $\tau_{\text{S}} = \tau_{\text{D}} + \epsilon$, where $\epsilon \ll \tau_{\text{D}}$. Then, we have

$$\frac{\tau_D}{2} \leqslant \tau_{dyn} \leqslant \left(\frac{\tau_D}{\epsilon}\right)\tau_D.$$

Depending on the size of ϵ, the upper bound on τ_{dyn} can be quite large. Thus, if the diffusion and reaction time scales are comparable, the dynamic time scale can be much larger than either of them.

3. Galerkin FE formulation

In this section a generic notation and representation of a reaction–diffusion PDE system is presented. This representation is used to develop the Galerkin weak form of the equations, as well as the discrete FEM formulation. This generalization also provides a consistent notation for the application of the various time integration strategies to the numerical test problems described in Section 5.

The system of N reaction–diffusion equations is solved in a bounded open region Ω in $\Re^d$, with $d = 1, 2,$ or 3, and Lipschitz continuous boundary $\partial\Omega = \Gamma_m \cup \Gamma_d$ over the time interval $(0, \Im]$. The reaction–diffusion equation is then

$$\frac{\partial \chi_i}{\partial t} + \nabla \cdot \mathbf{j}_i - S_i(\chi) = 0 \quad \text{in } \Omega \times (0, \Im] \tag{1}$$

for each unknown, χ_i, with the flux vector, $\mathbf{j}_i$, defined as

$$\mathbf{j}_i = -D_i \nabla \chi_i, \tag{2}$$

and $S_i(\chi)$ is a generic source term. The initial conditions are given by

$$\chi_i(\mathbf{x}, 0) = \chi_{0,i}(\mathbf{x}). \tag{3}$$

Dirichlet boundary conditions are defined on a portion of the boundary Γ_d,

$$\chi_i = g(\mathbf{x}) \quad \text{on } \Gamma_d, \tag{4}$$

as well as mixed or Robin boundary conditions on Γ_m for the remainder of $\partial\Omega$,

$$A\chi_i + B\mathbf{j}_i \cdot \mathbf{n} = C \quad \text{on } \Gamma_m. \tag{5}$$

The formal Galerkin weak form of the governing reaction–diffusion system is derived as follows. First, we define the spaces $H_0^1(\Omega) = \{\psi \in H^1(\Omega) | \psi = 0 \text{ on } \Gamma_d\}$ and $H_g^1(\Omega) = \{\psi \in H^1(\Omega) | \psi = g \text{ on } \Gamma_d\}$. Next we multiply Eq. (1) by a test function ϕ from the space $H_0^1(\Omega)$, which gives

$$\int_\Omega \phi \frac{\partial \chi_i}{\partial t}\, d\Omega + \int_\Omega \phi \nabla \cdot \mathbf{j}_i\, d\Omega - \int_\Omega \phi S_i(\chi)\, d\Omega = 0. \tag{6}$$

Using the Divergence theorem and flux definition from above, we obtain the resulting weak form

$$\int_\Omega \phi \frac{\partial \chi_i}{\partial t}\, d\Omega + \int_\Omega D_i \nabla \chi_i \cdot \nabla \phi\, d\Omega - \int_\Omega \phi S_i(\chi)\, d\Omega = -\int_{\Gamma_m} \phi \mathbf{j}_i \cdot \mathbf{n}\, d\Gamma \quad \forall \phi \in H_0^1(\Omega), \tag{7}$$

which can be summarized as follows. The weak form of the reaction–diffusion system is, for $t \in (0, \Im]$, to seek $\chi(\cdot, t) \in H_g^1(\Omega)$ such that

$$\mathscr{M}_i(\dot{\chi}, \phi) + \mathscr{D}_i(\chi, \phi) + \mathscr{S}_i(\chi, \phi) + \mathscr{F}_i(\phi) = 0 \quad \forall \phi \in H_0^1(\Omega), \tag{8}$$

where the forms $\mathscr{M}(\cdot,\cdot)$, $\mathscr{D}(\cdot,\cdot)$, $\mathscr{S}(\cdot,\cdot)$, and the functional $\mathscr{F}(\cdot)$ are the transient (or mass) operator,

$$\mathscr{M}_i(\dot{\chi}, \phi) = \int_\Omega \phi \frac{\partial \chi_i}{\partial t} \, \mathrm{d}\Omega, \tag{9}$$

the diffusion operator,

$$\mathscr{D}_i(\chi, \phi) = \int_\Omega D_i \nabla \chi_i \cdot \nabla \phi \, \mathrm{d}\Omega, \tag{10}$$

the reaction source term operator,

$$\mathscr{S}_i(\chi, \phi) = -\int_\Omega \phi S_i(\chi) \, \mathrm{d}\Omega, \tag{11}$$

and the boundary-flux operator,

$$\mathscr{F}_i(\phi) = \int_{\Gamma_m} \phi \mathbf{j}_i \cdot \mathbf{n} \, \mathrm{d}\Gamma. \tag{12}$$

A Galerkin FEM formulation for the generic reaction–diffusion equation restricts Eqs. (9)–(12) to the finite element spaces $\Phi^h \subset H^1(\Omega)$ and $\Phi_0^h \subset H_0^1(\Omega)$. The discrete problem then seeks $\chi^h \subset \Phi^h$ such that $\chi^h = g$ on Γ_d and

$$\mathscr{M}_i(\dot{\chi}^h, \phi^h) + \mathscr{D}_i(\chi^h, \phi^h) + \mathscr{S}_i(\chi^h, \phi^h) + \mathscr{F}_i(\phi^h) = 0 \quad \forall \phi^h \in \Phi_0^h. \tag{13}$$

In the discussion of the time integration schemes that follow, we further simplify the notation of Eq. (13) by dropping the explicit reference to the weighting function ϕ in the operators and suppressing the use of the superscript h.

4. Overview of time integration methods

4.1. Fully implicit methods

A fully implicit time integration of Eq. (13) evaluates all time-dependent terms at the next time level, $n+1$. We will consider two fully implicit methods. First, we have the first-order backward Euler method, referred to as FI-1,

$$\dot{\chi}^{n+1} = \frac{\chi^{n+1} - \chi^n}{\Delta t}. \tag{14}$$

Our second implementation is the second-order trapezoidal rule (FI-2(trap. rule))

$$\dot{\chi}^{n+1} = \frac{\chi^{n+1} - \chi^n}{\Delta t/2} - \dot{\chi}^n. \tag{15}$$

In general these methods will produce nonlinear algebraic equations for the solution at the new time step, which we solve using Newton's method.

The Generalized-α method is a parameterized family of methods that evaluates Eq. (13) as

$$\mathscr{M}_i(\dot{\chi}^{n+\alpha_m}) + \mathscr{D}_i^{n+\alpha_f}(\chi^{n+\alpha_f}) + \mathscr{S}_i^{n+\alpha_f}(\chi^{n+\alpha_f}) + \mathscr{F}_i^{n+\alpha_f} = 0. \tag{16}$$

For unconditional stability the parameters α_m and α_f must satisfy the stability condition [5,9]

$$\alpha_m \geqslant \alpha_f \geqslant \frac{1}{2}.$$

The intermediate values $\chi^{n+\alpha_f}$ and $\dot{\chi}^{n+\alpha_m}$ are given by

$$\chi^{n+\alpha_f} = (1-\alpha_f)\chi^n + \alpha_f \chi^{n+1},$$
$$\dot{\chi}^{n+\alpha_m} = (1-\alpha_m)\dot{\chi}^n + \alpha_m \dot{\chi}^{n+1}.$$

Intermediate times are similarly computed. A third coefficient, γ, relates χ and $\dot{\chi}$

$$\chi^{n+1} = \chi^n + \Delta t\left[(1-\gamma)\dot{\chi}^n + \gamma\dot{\chi}^{n+1}\right]. \tag{17}$$

For nonzero α_f, α_m, and γ this method will be implicit. The stability (robustness) of the implicit method is counter balanced by the requirement to solve large coupled systems of nonlinear equations. In addition, it should be noted that from the Generalized-α method it is possible to choose parameters such that a family of methods that transition from a second-order neutrally stable midpoint rule to a second-order BDF2 method is obtained. Further by introducing the parameter ρ_∞ with $0 \leqslant \rho_\infty \leqslant 1$, then setting

$$\alpha_f = \frac{1}{1+\rho_\infty}, \quad \alpha_m = \frac{1}{2}\left(\frac{3-\rho_\infty}{1+\rho_\infty}\right), \quad \gamma = \frac{1}{1+\rho_\infty},$$

guarantees that the resulting Generalized-α method will be second-order accurate and will damp high frequencies [9]. Note that the FI-1 and FI-2(trap. rule) methods can be considered special cases of this method, with $\alpha_m = \alpha_f = \gamma = 1$, and $\alpha_m = \alpha_f = 1$ and $\gamma = 1/2$, although these values do not correspond to values of ρ_∞. We will also consider the case $\rho_\infty = 0.8$ in our results, denoting it as FI-2($\rho_\infty = 0.8$). In our experience we found this method to have a desirable balance of accuracy and stability.

Additionally, we point out that all the implicit methods that we consider have the property that all the physical mechanisms (all terms with the exception of the time derivative) are evaluated at the same time level. We term this a balanced operator method, and use this terminology to differentiate between the splitting schemes that we introduce later.

4.2. Semi-implicit linearized methods

The semi-implicit linearized schemes that we consider are low-order expansions of the system at each time step to avoid the nonlinear iteration that is required by an implicit scheme. The price for this simplification is that while the resulting schemes are most often first-order, they are not, in general, unconditionally stable or balanced operator methods.

Lagged. A common first-order linearization technique known as lagging (SI-lagged) evaluates the nonlinear coefficients and source terms using values of the dependent variables at the last time step. The resulting system of equations can be described as

$$\mathscr{M}_i(\dot{\chi}^{n+1}) + \mathscr{D}_i^n(\chi^{n+1}) + \mathscr{S}_i^n(\chi^n) + \mathscr{F}_i^{n+1} = 0. \tag{18}$$

As defined above the SI-lagged scheme is not a balanced operator method.

Linearized. Here we chose a specific linearization of the source terms and the diffusion operator

$$\mathscr{M}_i(\dot{\chi}^{n+1}) + \mathscr{L}_{\mathscr{D}}\{\mathscr{D}_i^{n+1}(\chi^{n+1})\} + \mathscr{L}_{\mathscr{S}}\{\mathscr{S}_i^{n+1}(\chi^{n+1})\} + \mathscr{F}_i^{n+1} = 0, \tag{19}$$

and convert the nonlinear system into a linear system of equations that is solved at each time step. As an example for this case, a simple fixed-point linearization of the diffusion operator uses values at the last time step, n, to evaluate the diffusion coefficient, such as

$$\mathscr{L}_{\mathscr{D}}\{\mathscr{D}_i^{n+1}(\chi^{n+1})\} = \mathscr{D}_i^n(\chi^{n+1}) = \int_\Omega D_i^n \nabla \chi_i^{n+1} \cdot \nabla \phi \, \mathrm{d}\Omega. \tag{20}$$

In general, linearized methods will be first-order accurate and will be "non-balanced" operator methods, that is, the different physical terms are not converged at the same time level. For each problem we will define a particular linearization and refer to the resulting method as SI-linear 1. It should be noted that the linearized methods are not unique, so we will specify the linearization for each method.

A linearized method can be second-order accurate when $\mathscr{D}_i$, $\mathscr{S}_i$, and $\mathscr{F}_i$ have simple forms or are fully expanded to second order with exact derivatives. This latter case is the LIN2 algorithm of Lowrie [14] and will be referred to here as SI-linear 2. For systems with nonlinear diffusion or with source terms which cannot be expanded exactly to second order, this method can be approximated by using a numerical approximation to the Jacobian matrix. As shown in [18] for the radiation–diffusion problem, this can produce similar results to LIN2 by using a high accuracy linear solve and by stopping the Newton iteration after one step.

4.3. Operator-splitting methods

Operator-splitting schemes split the governing equations into sub-equations, usually with each having a single operator, and time integrate each separately and sequentially to advance to the next time step [15,30]. By construction these methods are non-balanced operator methods because the different operators are evaluated at different effective time levels. To motivate these methods and define a notation for further discussion, we first present a common first-order operator-splitting method.

First-order operator-splitting (FS). The classic two-step operator-splitting method splits the diffusion and reaction terms and solves them sequentially. We consider the case when the reaction terms are integrated first, followed by the diffusion terms. Advancing the solution from a solution at time level n to time level $n+1$ with a time-step size of Δt takes the form

$$\text{Step 1}: \quad \mathscr{M}_i(\dot{\chi}^*) + \mathscr{S}_i^*(\chi^*) = 0 \quad \text{on } [0,\Delta t], \quad \chi^*(\mathbf{x},0) = \chi^n(\mathbf{x}), \tag{21}$$

$$\text{Step 2}: \quad \mathscr{M}_i(\dot{\chi}^{**}) + \mathscr{D}_i^{**}(\chi^{**}) + \mathscr{F}_i^{**} = 0 \quad \text{on } [0,\Delta t], \quad \chi^{**}(\mathbf{x},0) = \chi^*(\mathbf{x},\Delta t), \tag{22}$$

where the next time-step value is $\chi^{n+1} = \chi^{**}(\Delta t)$. In the discussion that follows we denote the solution of the split-reaction step, Eq. (21), as $\chi^* = \tilde{S}_{\Delta t}\chi^n$ and the solution of the split-diffusion step, Eq. (22), as $\chi^{**} = \tilde{D}_{\Delta t}\chi^*$ and formally represent the first-order operator-splitting method as

$$\chi^{n+1} = \tilde{D}_{\Delta t}\tilde{S}_{\Delta t}\chi^n. \tag{23}$$

We should note that this operator-splitting method, referred to as FS-DR, can be second-order accurate if the operators, $\mathscr{D}_i$ and $\mathscr{S}_i$, commute (i.e., $\mathscr{D}_i\mathscr{S}_i = \mathscr{S}_i\mathscr{D}_i$) and if the solutions of Eqs. (21) and (22) are also second-order accurate [15]. Since we consider nonlinear equations and use first-order time integration for this splitting, we expect to obtain first-order asymptotic convergence rates. The FS-DR method can be reversed (FS-RD) as

$$\chi^{n+1} = \tilde{S}_{\Delta t}\tilde{D}_{\Delta t}\chi^n.$$

Sportisse [26] suggests that, for problems with a stiff and a non-stiff operator, the stiff operator should be evaluated last in the splitting sequence to increase the relative accuracy of the method.

Strang splitting (Strang). Strang's operator-splitting method [27] is a formally second-order scheme which applies a half-step of the reaction physics, a full-step of the diffusion physics, and finally another half-step of the reaction physics. This three-step operator-splitting method is

$$\text{Step 1}: \quad \mathscr{M}_i(\dot{\chi}^*) + \mathscr{S}_i^*(\chi^*) = 0 \quad \text{on } [0, \Delta t/2], \quad \chi^*(\mathbf{x}, 0) = \chi^n(\mathbf{x}),$$

$$\text{Step 2}: \quad \mathscr{M}_i(\dot{\chi}^{**}) + \mathscr{D}_i^{**}(\chi^{**}) + \mathscr{F}_i^{**} = 0 \quad \text{on } [0, \Delta t], \quad \chi^{**}(\mathbf{x}, 0) = \chi^*(\mathbf{x}, \Delta t/2),$$

$$\text{Step 3}: \quad \mathscr{M}_i(\dot{\chi}^{***}) + \mathscr{S}_i^{***}(\chi^{***}) = 0 \quad \text{on } [0, \Delta t/2], \quad \chi^{***}(\mathbf{x}, 0) = \chi^{**}(\mathbf{x}, \Delta t),$$

where the next time-step value is $\chi^{n+1} = \chi^{***}(\Delta t/2)$. Thus over the time step, Δt, all the diffusion and reaction physics have been integrated. Using the operator notation introduced earlier, we can write

$$\chi^{n+1} = \tilde{S}_{\Delta t/2}\tilde{D}_{\Delta t}\tilde{S}_{\Delta t/2}\chi^n. \tag{24}$$

We refer to this method as Strang RDR. As with FS-DR, the reaction and diffusion steps in Strang splitting can be switched (Strang DRD) as

$$\chi^{n+1} = \tilde{D}_{\Delta t/2}\tilde{S}_{\Delta t}\tilde{D}_{\Delta t/2}\chi^n \tag{25}$$

to reduce the size of the diffusion time step from Δt to $\Delta t/2$. It should be noted that for formal second-order accuracy the component solves must be at least second-order accurate.

Romero splitting (Romero). The Romero splitting technique [21] is a formally second-order method that is similar to Strang DRD. However, this technique uses first-order solves for the diffusion steps. In addition the Romero splitting solves the diffusion terms with alternating explicit and implicit solves

$$\chi^{n+1} = \tilde{D}^{\text{imp}}_{\Delta t/2}\tilde{S}_{\Delta t}\tilde{D}^{\text{exp}}_{\Delta t/2}\chi^n. \tag{26}$$

In our case we use forward and backward Euler for the diffusion sub-problem. In general, Romero splitting assumes that the reaction has a fast time scale compared to the diffusion, and that the reaction sub-problem can be solved exactly. However in practice, non-exact numerical solutions to the reaction sub-problem still produce second-order solutions in our studies. Over two successive time steps, the first-order implicit solve is followed by the first-order explicit solve. Intuitively, the combination of these two solves, sequentially, produces a classic second-order central difference approximation if the time-step sizes are the same.

4.4. Efficient FE splitting methods

In order to motivate the development of efficient FE operator-splitting methods for our problems, we consider the reaction step of a generic operator-splitting method. In the reaction step, the system

$$\mathscr{M}_i(\dot{\chi}^*) + \mathscr{S}_i^*(\chi^*) = 0, \tag{27}$$

must be solved with suitable initial conditions over the appropriate time interval. In the case of a FE method, this system would produce a large sparse nonlinear system of equations of dimension $N = N_{\text{unknowns}} \times N_{\text{nodes}}$. In general this would be expensive to solve but could be accomplished with a suitable method. However, this methodology would appear to be somewhat inconsistent with the standard operator-splitting philosophy of efficient component solves for each of the respective operators. It can be easily shown that an alternate approach which employs a group FE expansion [8] for this system reduces Eq. (27) to a system of ODEs of dimension $N = N_{\text{unknowns}}$, to be solved at each node of the FE mesh. In practice we implement the solution of this local ODE system with a stiff ODE solver (see Section 6.1.1) and employ very strict error tolerances to minimize error accumulation over the intermediate reaction time step.

5. Description of test problems

In this section, we present a description of the four test problems that are used to numerically evaluate the relative accuracy and asymptotic order of accuracy of the time integration techniques described above. In addition to the description of the test problems, initial conditions and boundary conditions, we also present the operator-specific linearizations that are used in the first-order semi-implicit linearized (SI-linear 1) time integration technique.

5.1. Thermal wave

The first test problem that we will describe is associated with the solution to the time-dependent heat equation with a nonlinear source term. This test problem of Knio et al. [10] provides a numerical example with a smooth analytic solution in the form of a propagating wave. The nonlinear reaction–diffusion equation is

$$\frac{\partial T}{\partial t} = \frac{\partial^2 T}{\partial x^2} + \frac{8}{\delta^2} T^2 (1 - T), \tag{28}$$

where the boundary conditions are $T(x = -\infty, t) = 1$ and $T(x = \infty, t) = 0$. The parameter, $\delta > 0$, can be freely selected but does not change the ratio of time scales between the diffusion and the reaction terms. The analytic solution is

$$T(x,t) = \frac{1}{2}\left(1 - \tanh\left[\frac{x - 2t/\delta}{\delta}\right]\right), \tag{29}$$

where we have selected $\delta = 1$.

This one-dimensional problem is modeled with linear elements in the finite element mesh, covering the domain $-10 \leqslant x \leqslant 10$. The simulation was integrated to $t_{\text{final}} = 1.024$ with mesh spacings of $\Delta x = 0.005$ and $\Delta x = 0.04$. Since the solution is a wave front with a speed of $c = 2$, we use the CFL condition to define a characteristic time scale of $\tau = \Delta x/c = 0.02$ for the coarse discretization and $\tau = 0.0025$ for the fine discretization.

We can relate the thermal wave problem with the general reaction–diffusion formulation (i.e., Eqs. (8)–(12)) as follows:

$$\chi = T,$$

$$\mathbf{j}_i = -D_i \nabla \chi_i = -\nabla T,$$

$$\mathscr{D}_i^{n+1}(\chi^{n+1}) = \int_\Omega \nabla T^{n+1} \cdot \nabla \phi \, \mathrm{d}\Omega,$$

$$\mathscr{S}_i^{n+1}(\chi^{n+1}) = -\int_\Omega \frac{8}{\delta^2} (T^{n+1})^2 (1 - T^{n+1}) \phi \, \mathrm{d}\Omega.$$

For the SI-linear 1 runs, the source term linearization is a simple fixed-point linearization of $\mathscr{S}(T)$ such that

$$\mathscr{L}_{\mathscr{S}}\{\mathscr{S}_i^{n+1}(\chi^{n+1})\} = -\int_\Omega \frac{8}{\delta^2} T^{n+1} T^n (1 - T^n) \phi \, \mathrm{d}\Omega. \tag{30}$$

Since the diffusion coefficient is constant, no linearization of the diffusion operator is required. The SI-linear 2 method is based on trapezoidal rule and a straight-forward Taylor series expansion of the source term to second order.

5.2. Brusselator

The next test case is the Brusselator problem, a coupled set of equations first introduced by Prigogine and Lefever [20] as a model of chemical dynamics. They are

$$\frac{\partial T}{\partial t} = D_1 \frac{\partial^2 T}{\partial x^2} + \alpha - (\beta + 1)T + T^2 C, \tag{31}$$

$$\frac{\partial C}{\partial t} = D_2 \frac{\partial^2 C}{\partial x^2} + \beta T - T^2 C, \tag{32}$$

with the boundary conditions $T(0,t) = T(1,t) = \alpha$ and $C(0,t) = C(1,t) = \beta/\alpha$. These equations admit steady state, oscillatory and chaotic solutions. In our studies we consider parameter values of $\alpha = 0.6$, $\beta = 2$, and $D_i = 1/40$ for $i = 1$ and 2 which produce an oscillatory solution. Analysis of this problem can be found in [21].

This coupled system was modeled with linear elements with a grid spacing of $\Delta x = 0.002$. The system was integrated to times of $t = 6.4$, 16, 32, 64, and 80, using time steps ranging from 3.2 to 7.8×10^{-3}. For a characteristic time scale we use the period of oscillation of the solution, which we found experimentally to be $\tau = 12$.

The identification of the Brusselator problem with the general reaction–diffusion form of Eqs. (8)–(12) is given as

$$\chi = [T, C]^{\mathrm{T}},$$

$$\mathbf{j}_i = -D_i \nabla \chi_i = \begin{cases} -D_1 \nabla T & \text{for } i = T, \\ -D_2 \nabla C & \text{for } i = C, \end{cases}$$

$$\mathscr{D}_i^{n+1}(\chi^{n+1}) = \begin{cases} \int_\Omega D_1 \nabla T^{n+1} \cdot \nabla \phi \, \mathrm{d}\Omega & \text{for } i = T, \\ \int_\Omega D_2 \nabla C^{n+1} \cdot \nabla \phi \, \mathrm{d}\Omega & \text{for } i = C, \end{cases}$$

$$\mathscr{S}_i^{n+1}(\chi^{n+1}) = \begin{cases} -\int_\Omega \left[\alpha - (\beta+1)T^{n+1} + (T^{n+1})^2 C^{n+1}\right] \phi \, \mathrm{d}\Omega & \text{for } i = T, \\ -\int_\Omega \left[\beta T^{n+1} - (T^{n+1})^2 C^{n+1}\right] \phi \, \mathrm{d}\Omega & \text{for } i = C. \end{cases}$$

The linearization of the source-term operator for SI-linear 1 is defined as

$$\mathscr{L}_{\mathscr{S}}\{\mathscr{S}_i^{n+1}(\chi^{n+1})\} = \begin{cases} -\int_\Omega \left[\alpha - (\beta+1)T^{n+1} + \frac{T^n}{2}(T^{n+1}C^n + T^n C^{n+1})\right] \phi \, \mathrm{d}\Omega & \text{for } i = T, \\ -\int_\Omega \left[\beta T^{n+1} - \frac{T^n}{2}(T^{n+1}C^n + T^n C^{n+1})\right] \phi \, \mathrm{d}\Omega & \text{for } i = C. \end{cases} \tag{33}$$

This linearization is a simple choice of a fixed-point linearization which averages the contributions from the cross-coupling source term. The SI-linear 2 method is based on a straight-forward Taylor series expansion of the source term to second order.

5.3. Blow-up

The third test case is a model of a blow-up problem. The two special cases consider linear and nonlinear diffusion. This scalar equation can exhibit unbounded growth in finite time. The equation is

$$\frac{\partial T}{\partial t} = \beta \frac{\partial}{\partial x}\left(D(T)\frac{\partial T}{\partial x}\right) + T^2, \tag{34}$$

with the boundary conditions

$$T(0,t) = T(1,t) = 0. \tag{35}$$

If the value of β is sufficiently low and the initial conditions are sufficiently large, the solutions of this equation will exhibit blow-up in finite time. Surveys of work on these equations can be found in [1,23].

We considered two cases: linear diffusion (LD), with $D = 1$ and $\beta = 0.05$; and nonlinear diffusion (ND), with $D = T$ and $\beta = 0.1$. For both of these cases the initial profile is

$$T(x,0) = 4x(1-x),$$

a parabola with height 1. For each problem, the combination of initial condition and diffusion term enables blow-up to occur in a finite time.

For each case the mesh spacing was $\Delta x = 0.002$ and the integration was carried out until the solution reached blow-up, i.e., either the solution became infinite or the nonlinear solver could not converge, or until the solution became unphysical, either by becoming negative or by developing oscillations.

Runs of the blow-up problem with linear diffusion (LD) indicated that blow-up occurred near $t = 1.57$, while those of the blow-up problem with nonlinear diffusion (ND) suggested a blow-up time near $t = 2.35$. Thus, we use these times as the characteristic time scales for these problems.

We can relate the blow-up problem with the general reaction–diffusion formulation (i.e., Eqs. (8)–(12)) as follows:

$$\chi = T,$$

$$\mathbf{j}_i = -\beta D(\chi)\nabla\chi_i = -\beta D(T)\nabla T,$$

$$\mathscr{D}_i^{n+1}(\chi^{n+1}) = \beta \int_\Omega D\left(T^{n+1}\right)\nabla T^{n+1}\cdot\nabla\phi,$$

$$\mathscr{S}_i^{n+1}(\chi^{n+1}) = -\int_\Omega \left(T^{n+1}\right)^2\phi \, \mathrm{d}\Omega.$$

For the SI-linear 1 runs, the diffusion and source-term linearization is a simple fixed-point linearization such that

$$\mathscr{L}_{\mathscr{D}}\{\mathscr{D}_i^{n+1}(\chi^{n+1})\} = \beta \int_\Omega D(T^n)\nabla T^{n+1}\cdot\nabla\phi \, \mathrm{d}\Omega, \tag{36}$$

$$\mathscr{L}_{\mathscr{S}}\{\mathscr{S}_i^{n+1}(\chi^{n+1})\} = -\int_\Omega T^{n+1}T^n\phi \, \mathrm{d}\Omega. \tag{37}$$

The SI-linear 2 method for the blow-up (LD) problem is based on a straight-forward Taylor series expansion of the source term to second order.

5.4. Non-equilibrium radiation diffusion

The non-equilibrium radiation–diffusion problem is defined by a nonlinear coupled set of equations with a solution that contains a very sharp gradient and discontinuous first derivative at the wavefront. The governing equations for the non-equilibrium radiation–diffusion approximation are given by

$$\frac{\partial E}{\partial t} - \frac{\partial}{\partial x}\left(cD_{\mathrm{r}}\frac{\partial E}{\partial x}\right) = c\sigma_{\mathrm{a}}\left(aT^4 - E\right) \quad \text{in } \Omega, \tag{38}$$

$$\frac{\partial(C_{\mathrm{v}}T)}{\partial t} = -c\sigma_{\mathrm{a}}\left(aT^4 - E\right) \quad \text{in } \Omega, \tag{39}$$

and are solved in the domain $\Omega = [0,1]$ for $t \in (0,1]$, where E is the radiation energy density, T is the material temperature, c is the speed of light, D_{r} is the radiation–diffusion coefficient, σ_{a} is the inverse absorption mean free path, $a = 4\sigma_{\mathrm{SB}}$ where σ_{SB} is the Stefan–Boltzmann constant, and C_{v} is the material heat capacity. Following [12] a system of units has been selected so that $C_{\mathrm{v}} = c = a = 1$, and the initial conditions are

$$E(x,0) = E_0(x) \quad \text{in } \Omega, \tag{40}$$

$$T(x,0) = T_0(x) \quad \text{in } \Omega, \tag{41}$$

where $E_0(x) = 10^{-5}$ and $T_0(x) = E_0(x)^{1/4}$. The boundary conditions are of mixed type and can be written as

$$AE + B(\mathbf{j}\cdot\mathbf{n}) = C \quad \text{on } \partial\Omega \ \forall t, \tag{42}$$

where $A = 1/4$, $B = -1/2$, and $C = 1$ for $x = 0$; and $A = 1/4$, $B = 1/2$, and $C = 0$ for $x = 1$.

The absorption cross-section is modeled by $\sigma_{\mathrm{a}} = T^{-3}$, and the diffusion coefficient is $D_{\mathrm{r}} = 1/(3\sigma_{\mathrm{a}})$ from simple isotropic theory. However in regions of strong gradients, the theory can fail and allow the flux of energy to move faster than the speed of light. A flux-limiting can be applied to D_{r} to prevent this unphysical behavior, and we use [4,12,13,16]

$$D_{\mathrm{r}} = \frac{1}{3\sigma_{\mathrm{a}} + \frac{1}{E}\left|\frac{\partial E}{\partial x}\right|}. \tag{43}$$

We use a spatial discretization of $\Delta x = 0.005$. The approximate observed wave speed is $c = 0.4$. As with the Thermal Wave problem, we define the characteristic time scale as $\tau = \Delta x/c = 0.0125$.

The identification of the radiation–diffusion problem with the general reaction–diffusion form of Eqs. (8)–(12) is given as

$$\chi = [E,T]^{\mathrm{T}},$$

$$\mathbf{j}_i = -D_i\nabla\chi_i = \begin{cases} -D_{\mathrm{r}}\nabla E & \text{for } i = E, \\ 0 & \text{for } i = T, \end{cases}$$

$$\mathscr{D}_i^{n+1}(\chi^{n+1}) = \begin{cases} \int_\Omega D_{\mathrm{r}}^{n+1}\nabla E^{n+1}\cdot\nabla\phi \,\mathrm{d}\Omega & \text{for } i = E, \\ 0 & \text{for } i = T, \end{cases}$$

$$\mathscr{S}_i^{n+1}(\chi^{n+1}) = \begin{cases} -\int_\Omega \phi\sigma^{n+1}\left[\left(T^{n+1}\right)^4 - E^{n+1}\right]\mathrm{d}\Omega & \text{for } i = E, \\ \int_\Omega \phi\sigma^{n+1}\left[\left(T^{n+1}\right)^4 - E^{n+1}\right]\mathrm{d}\Omega & \text{for } i = T. \end{cases}$$

The linearization of the diffusion and source-term operators for SI-linear 1 is defined as

$$\mathscr{L}_{\mathscr{D}}\{\mathscr{D}_i^{n+1}(\chi^{n+1})\} = \begin{cases} \int_\Omega D_{\mathrm{r}}^{n}\nabla E^{n+1}\cdot\nabla\phi \,\mathrm{d}\Omega & \text{for } i = E, \\ 0 & \text{for } i = T, \end{cases} \tag{44}$$

$$\mathscr{L}_{\mathscr{S}}\{\mathscr{S}_i^{n+1}(\chi^{n+1})\} = \begin{cases} -\int_\Omega \phi\sigma^n \left[(T^n)^3 T^{n+1} - E^{n+1}\right]\phi \, \mathrm{d}\Omega & \text{for } i = E, \\ \int_\Omega \phi\sigma^n \left[(T^n)^3 T^{n+1} - E^{n+1}\right] \mathrm{d}\Omega & \text{for } i = T. \end{cases} \tag{45}$$

The SI-linear 2 method is approximated by a one-step Newton method because of the difficulties of producing exact second-order expansions.

6. Numerical solutions

In this section, we give an overview of the implementation of the numerical methods, particularly the time level advancement and the selection of reference solutions. All the tolerances in this study were selected to be very restrictive to eliminate uncontrolled sources of errors from entering into the comparisons of the relative accuracy and asymptotic order of accuracy studies. In practice the tolerances are unnecessarily restrictive for normal computational simulations; however we used them as a means of obtaining careful estimates of the errors of the particular time integration methods of interest. As remarked earlier, studies that consider the efficiency of solving these systems of equations can be found in [4,12].

6.1. Solution methods

Solutions were obtained using FEMLAB, a finite element method (FEM) software package based on MATLAB for solving a variety of partial differential equations. Details on how this was implemented comprise the remainder of this section.

While the spatial discretization of the equations was done within FEMLAB using linear elements, the time integration was performed using our own time integrators, which we implemented within MATLAB. The implementations of these were based on the MATLAB ODE integration routines, particularly `ode23t` [25]. Linear solves were usually performed with the MATLAB backslash operator which uses Cholesky factorization for positive definite matrices or LU factorization for square nonsingular (but not positive definite) matrices. The only exceptions were cases where the same matrix was inverted multiple times, in which case the LU factors were saved and used as needed. Nonlinear solves were performed using Newton iteration.

The source terms were integrated using a node-based quadrature. In this method, rather than evaluating the source terms at the Gauss points, they are evaluated at the nodes and linearly interpolated to the Gauss points. This was done to conform to the practice of production codes such as MPSalsa [24], where it is implemented to speed up evaluation of these terms. The difference between solutions using standard Gauss quadrature and those using this nodal quadrature is small and scales as Δx^2. Moreover, using this quadrature allowed for a good comparison between the split and non-split methods at a coarser grid than would have been possible if Gauss quadrature had been used.

The radiation–diffusion test case is an exception to the above procedure. It was solved using MPSalsa, a code for simulating reacting flows. Details as to how it was implemented can be found in [18]. We note that in order to control oscillations near the sharp gradient at the wavefront, the mass and source terms had to be lumped in the fully implicit methods.

In each of the time integration methods the time step was kept constant throughout each run except for in two situations. The first is during the start-up phase, when the time step was ramped up. This is necessary for second-order methods, if they are initiated with a first-order method, so that they can maintain second-order accuracy. It was also found necessary for the blow-up (ND) problem so that the initial condition could develop into a suitable solution profile. The other situation was when the nonlinear solver could not converge. Then, the time step would be halved and the problem solved with the new time step. The time step

would then be doubled to return to the specified time step. A complete explanation of these procedures can be found in [18].

6.1.1. ODE solver

As mentioned in Section 4.4, the reaction step of an operator-splitting method can be solved as a system of ODEs at each node. These ODE equations are time integrated using the CVODE library [6]. In CVODE the following options are used: (1) backward differentiation formula (BDF) for the time advancement, (2) Newton iteration for the nonlinear solves, (3) a direct method with a banded treatment of the Jacobian where the Jacobian is formed analytically, (4) normal mode where smaller time steps can be taken (i.e., subcycling) to obtain the solution at the next time step, $n+1$, and (5) the relative and absolute error tolerances of the maximum of 10^{-12} and 10^{-14}. In our studies we selected these tolerances to minimize the accumulation of error in the ODE reaction solve. If less strict tolerances are employed the split schemes can be observed to stagnate in the convergence plots as the accumulated errors in the ODE solver destroy the convergence to the reference solution for the smallest overall time step sizes.

6.2. Solution comparison

To compare the accuracy of the various methods, we use a relative L_2 norm of the error, similar to that found in [18]. The relative L_2 error norm is defined as the ratio of the L_2 norm of the error to the L_2 norm of the reference solution. Each L_2 norm is a summation over all the unknowns, indexed by v, of the component L_2 norms:

$$\left\|\chi-\chi^{\mathrm{ref}}\right\| = \frac{\sum_i \left[\int |\chi_i - \chi_i^{\mathrm{ref}}|^2 \,\mathrm{d}x\right]^{1/2}}{\sum_i \left[\int |\chi_i^{\mathrm{ref}}|^2 \mathrm{d}x\right]^{1/2}}.$$

These integrals can be computed if we express χ and χ^{ref} in terms of the finite element basis functions. By normalizing the L_2 norm of the error, the relative differences in scaling (magnitude) between the unknowns, χ_{v}, are accounted for and the error of one unknown does not dominate.

For the blow-up problems, the time that the solution reaches a particular value can be important. Thus, we also consider convergence of the time that the maximum value of the solution reaches a reference temperature. For certain systems, this reference temperature may be an ignition temperature. Because the solution may not reach the reference temperature exactly, we determine the time interval during which the solution passed the reference temperature, and then use a cubic spline over six solution times to determine the time that the reference temperature was attained. The cubic spline interpolation is of higher-order accuracy than the time integration methods so as to not effect the numerical accuracy of the results. The error that we report is then

$$\left\|t-t^{\mathrm{ref}}\right\| = \frac{|t-t^{\mathrm{ref}}|}{|t^{\mathrm{ref}}|}.$$

6.3. Reference solutions

Any discrete numerical approximation of a time-dependent PDE will produce both spatial and temporal discretization errors in the numerical solution. To determine the relative magnitude of these errors and to estimate the order of accuracy of the individual methods, it is possible to carry out numerical convergence studies. These studies are based on an expansion of the numerical solution about the exact solution to a

leading order in the space (Δx) and time (Δt) discretization parameters. In this section, we state the error models that form the basis for these numerical studies.

From FEM theory for transient nonlinear parabolic problems [17,29], we expect the global error between the numerical solution and the exact solution to be characterized by

$$\|\chi - \chi^{\text{exact}}\| = \mathrm{o}(\Delta x^p) + \mathrm{o}(\Delta t^q),$$

where p is the asymptotic spatial order of accuracy, and q is the asymptotic temporal order of accuracy. We formally assume that we can represent the global error as

$$e = \|\chi - \chi^{\text{exact}}\| = C_x \Delta x^p + C_t \Delta t^q, \tag{46}$$

where in the asymptotic region of convergence both, C_x and C_t, are independent of Δx and Δt. We further assume that, to lowest order, a point-wise asymptotic error expansion of the type

$$\chi = \chi^{\text{exact}} + \tilde{C}_x \Delta x^p + \tilde{C}_t \Delta t^q + R(\chi) \tag{47}$$

holds for a sufficiently regular exact solution where $R(\chi)$ represents the higher-order terms and the expansion coefficients are again assumed to be independent of the temporal and spatial mesh sizes. The numerical studies that follow will support these assumptions.

An estimate of the discretization errors can be determined by comparing against a suitable reference solution, $\tilde{e} = \|\chi - \chi^{\text{ref}}\|$. The present study employs an extrapolated solution based on Richardson extrapolation, as in [18].

A temporal-extrapolated solution can be formed from a simple Richardson extrapolation procedure (see [22]) which relies on the point-wise expansion described above. The expansions for two solutions at different time resolutions (subscripts indicate resolution levels), neglecting higher-order terms, are

$$\chi_i = \chi^{\text{exact}} + \tilde{C}_x \Delta x^p + \tilde{C}_t \Delta t_i^q,$$

$$\chi_j = \chi^{\text{exact}} + \tilde{C}_x \Delta x^p + \tilde{C}_t \Delta t_j^q.$$

Define the temporal-extrapolated solution as the exact solution plus the spatial error

$$\chi^{\text{extrap}} \equiv \chi^{\text{exact}} + \tilde{C}_x \Delta x^p.$$

Using the above relations we can solve for the extrapolated solution

$$\chi^{\text{extrap}} = \chi_j + (\chi_j - \chi_i)/(r_{ij}^q - 1), \tag{48}$$

where $r_{ij} = \Delta t_i / \Delta t_j$. If the extrapolated solution of Eq. (48) is used as the reference solution, the global error is

$$\tilde{e}_i = \left\|\chi_i - \chi_j^{\text{extrap}}\right\| = \left\|\tilde{C}_t\right\| \Delta t_i^q = \tilde{\tilde{C}}_t \Delta t_i^q.$$

Again the spatial errors have canceled out, leaving only the temporal errors, $\tilde{\tilde{C}}_t \Delta t_i^q$ and higher-order terms. However, the temporal order of accuracy, q, in Eq. (48) must be selected in order to obtain the extrapolated solution (i.e., $q = 1$ for first-order or $q = 2$ for second-order time integration). If q is unknown, an iteration is required between the estimated $\tilde{q}$ and the generation of χ^{extrap} until the estimated $\tilde{q}$ matches the actual asymptotic order q. An alternative approach is to compute an apparent order of accuracy, $\tilde{q}$, which can be obtained using three numerical solutions, (χ_i, χ_j, χ_k) [22].

In practice we will assume that, for each method, q is the formal order of accuracy, and we will use the above procedure to determine a reference solution for each problem and spatial discretization. We will use

the FI-2($\rho_\infty = 0.8$) method in determining the reference solution except where noted. For the blow-up problems we also use this method to determine a reference time at which the solution reaches the reference temperature. The exception to this procedure is the subset of the spatial convergence studies that exhibited non-optimal convergence rates due to nearly discontinuous spatial solutions, in particular, the blow-up (ND) and radiation–diffusion problems. In these cases extrapolation method did not work well for producing reference solutions. For this reason we have employed the finest computed resolution solutions (i.e., smallest Δx) as the reference solution for all the spatial convergence studies. In the spatial convergence cases that do achieve optimal rates, this method is shown to qualitatively produce the expected rate of convergence. The drawback of this methodology is that the convergence rate between the finest two values of Δx plotted is slightly greater than the actual order; for more discussion of this behavior and alternate methods to calculate the actual obtained order of accuracy see [18].

7. Numerical experiments

7.1. Thermal wave

A plot of the thermal wave solution is shown in Fig. 1. As expected, it maintains the original smooth profile and propagates to the right with a constant speed. The spatial convergence of the thermal wave is shown in Fig. 2, where we have used the FI-2($\rho_\infty = 0.8$) method with $\Delta t = 0.0005$. The figure presents the relative L_2 error norm compared to a reference solution using $\Delta x = 0.0025$. As expected, the linear finite elements exhibit second-order convergence in Δx. The other methods display similar behavior. Thus, we are in the asymptotic regime in terms of the spatial error.

In Fig. 3 we show the temporal convergence, plotting the relative L_2 error norm against Δt for all the methods. The reference solution is computed by taking the two solutions with smallest time steps using the FI-2($\rho_\infty = 0.8$) method, and using Richardson extrapolation, assuming the formal order of temporal convergence. For both grids, all the methods exhibit their asymptotic rate of convergence, either first- or second-order.

Among the methods the SI-lagged technique is always the least accurate, although FI-1 is very close to it for the fine grid. Of the other first-order methods the accuracy (i.e., $\tilde{\tilde{C}}_t$) appears to depend on the spatial

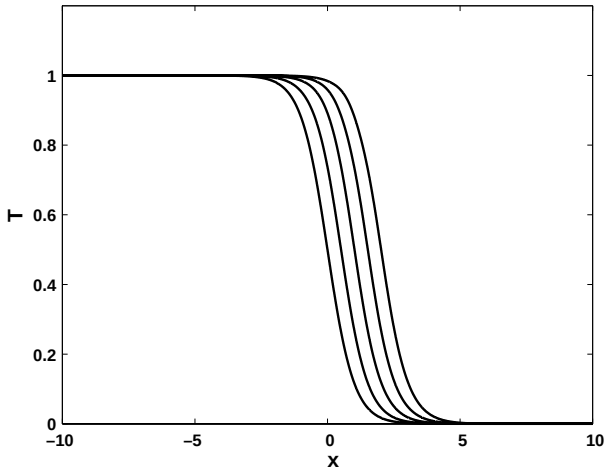

Fig. 1. Thermal wave profiles at $t = 0$, 0.256, 0.512, 0.768, and 1.024. Solution computed using FI-2($\rho_\infty = 0.8$) with $\Delta t = 0.0005$.

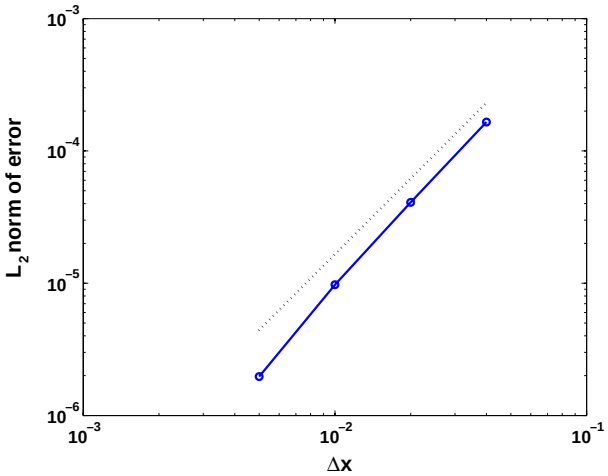

Fig. 2. Thermal wave spatial convergence using FI($\rho_\infty = 0.8$) with $\Delta t = 0.0005$. Reference solution uses $\Delta x = 0.0025$.

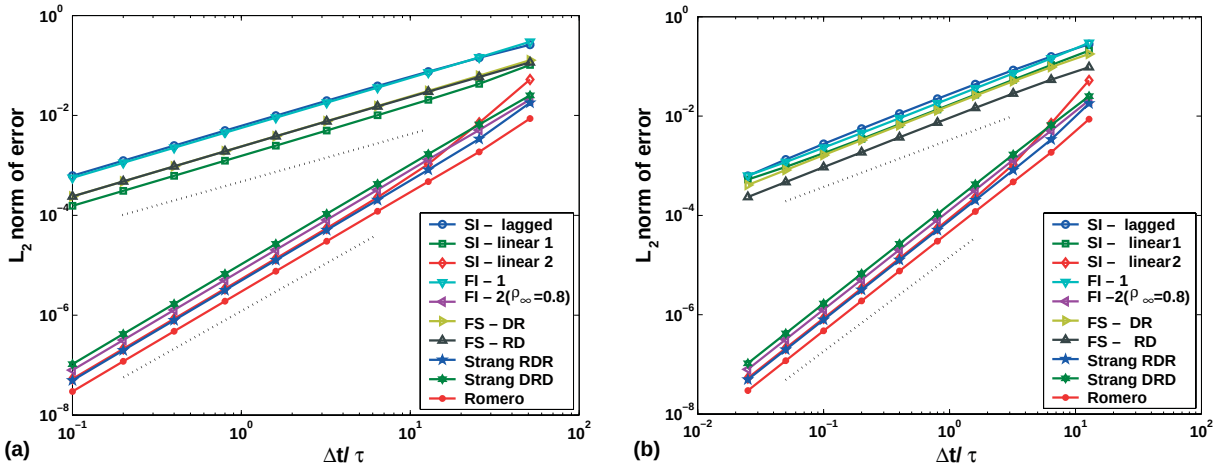

Fig. 3. Thermal wave temporal convergence with (a) $\Delta x = 0.005$ and (b) $\Delta x = 0.04$. The dotted lines are references with first- and second-order slopes.

resolution. For both spatial resolutions the errors for first-order methods vary by an order of magnitude. Alternatively, for a specified error the least accurate method requires a time step an order of magnitude smaller than the most accurate method.

The most accurate of the second-order methods is Romero, followed by Strang RDR, SI - linear 2, FI-2($\rho_\infty = 0.8$), and Strang DRD. This ordering appears to be independent of spatial resolution. The higher accuracy of the operator-splitting methods is likely due to higher accuracy solve in CVODE for the non-linear reaction term and appears to have offset the splitting errors for these methods.

For a fixed Δt, the errors of the first-order methods vary by an order of magnitude, as do the second-order methods. For a fixed error tolerance this corresponds to time steps ranging by an order of magnitude between the most accurate and least accurate first-order methods and even less between the most and least

accurate second-order methods. If we compare the least accurate first-order method (SI-lagged) with the most accurate second-order method (Romero), we see that for an error of 10^{-4}, SI-lagged requires a time step which is approximately two orders of magnitude smaller than the time step that Romero requires, while for a time step of 2×10^{-3} the error ranges over three orders of magnitude.

7.2. Brusselator

Fig. 4 shows the L_2 norm of the spatial error of the Brusselator solution at $t = 80$ using Strang DRD with $\Delta t = 0.0016$. The reference solution is a similar run with $\Delta x = 0.0005$. This plot shows that the second-order convergence in Δx is achieved, and that we are within the asymptotic range for spatial convergence.

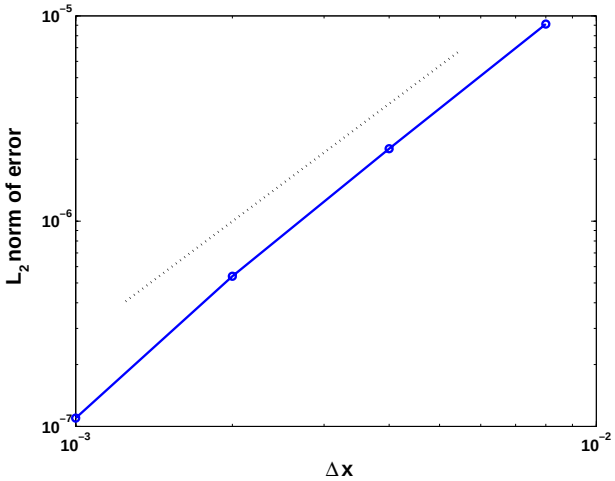

Fig. 4. Brusselator spatial convergence using Strang (DRD) L_2 norm of the error, $t = 80$, $\Delta t = 0.0016$. Reference solution uses $\Delta x = 0.0005$. The dotted line is a reference with a second-order slope.

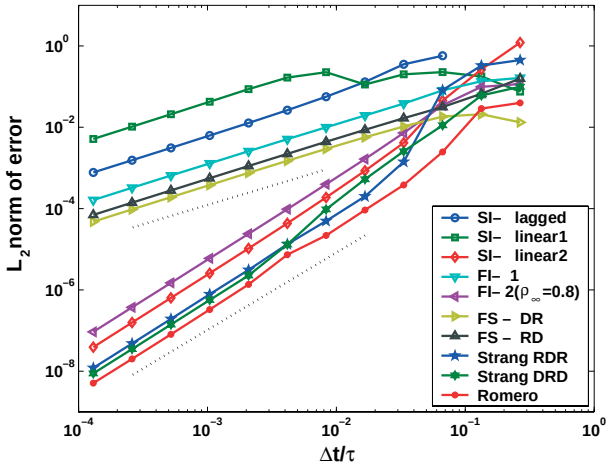

Fig. 5. Brusselator temporal convergence at $t = 16$. The dotted lines are references with first- and second-order slopes.

In Figs. 5–7, we present the temporal convergence of all the methods at the times $t = 16$, 64, and 80. We see that the first-order methods all exhibit first-order convergence and, except at larger time steps, are in their asymptotic convergence regime, although SI-linear 1 requires a small Δt for correct convergence. Around $\Delta t = 3 \times 10^{-3}$, the range of errors between the most accurate and least accurate first-order methods can be up to an order of magnitude. The split methods are the most accurate, followed by FI-1, SI-lagged, and SI-linear 1.

Among the second-order methods, the SI-linear 2 and FI-2($\rho_\infty = 0.8$) methods show second-order convergence. For the second-order operator-splitting methods, the situation is considerably different. For $t = 16$ the convergence of these methods looks fine and they appear to be even more accurate than the non-split method. At $t = 64$, though, these methods are producing larger errors for larger values of the time

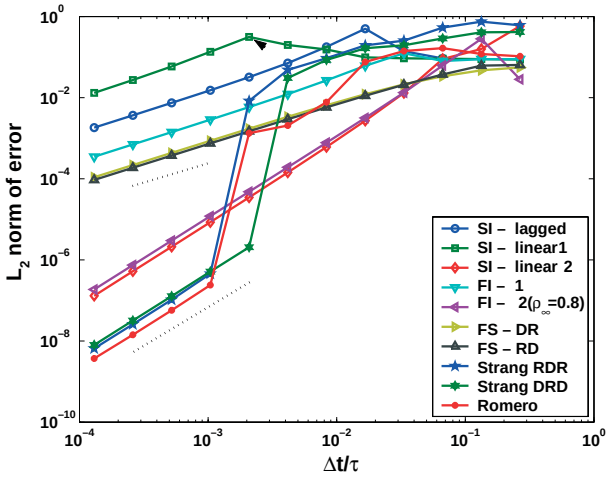

Fig. 6. Brusselator temporal convergence at $t = 64$. The dotted lines are references with first- and second-order slopes.

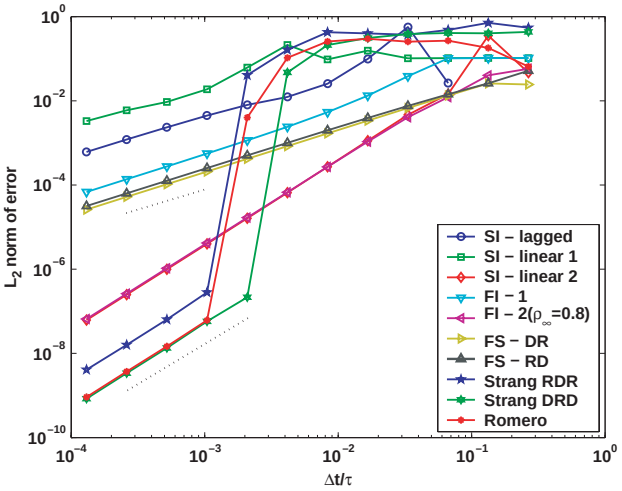

Fig. 7. Brusselator temporal convergence at $t = 80$. The dotted lines are references with first- and second-order slopes.

step. These errors grow, until at $t = 80$ these methods have nearly O(1) error for $\Delta t > 0.02$. At $\Delta t = 0.0125$ for Strang RDR and Romero and $\Delta t = 0.025$ for Strang DRD, there is sudden change, however, and the methods' errors drop below the level of errors of the non-split method and exhibit second-order convergence.

In Figs. 8–10, we show this effect again, but have grouped together different solution run-times of each method. Fig. 8 shows the temporal convergence for the FI-2($\rho_\infty = 0.8$) method for $t = 6.4$, 16, 32, 64, and 80. For $\Delta t \leqslant 0.8$, this method shows second-order temporal convergence at each time. Figs. 9 and 10 show the temporal convergence for Strang DRD and Romero splitting. In each of these cases the error for runs

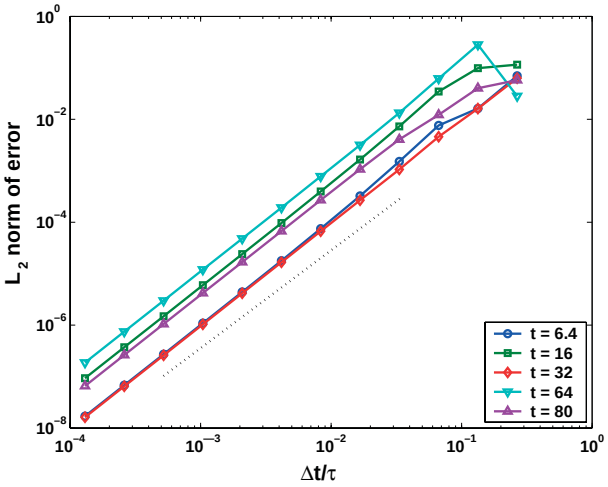

Fig. 8. Brusselator temporal convergence using Generalized-α ($\rho_\infty = 0.8$) with $\Delta x = 0.002$. The dotted line is a reference with second-order slope.

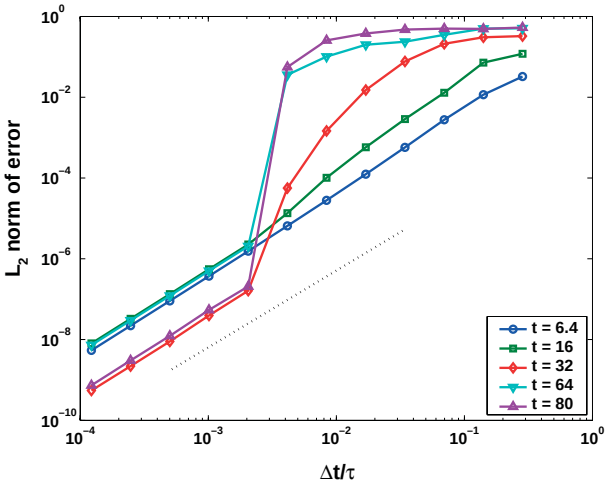

Fig. 9. Brusselator temporal convergence using Strang splitting (DRD) L_2 with $\Delta x = 0.002$. The dotted line is a reference with second-order slope.

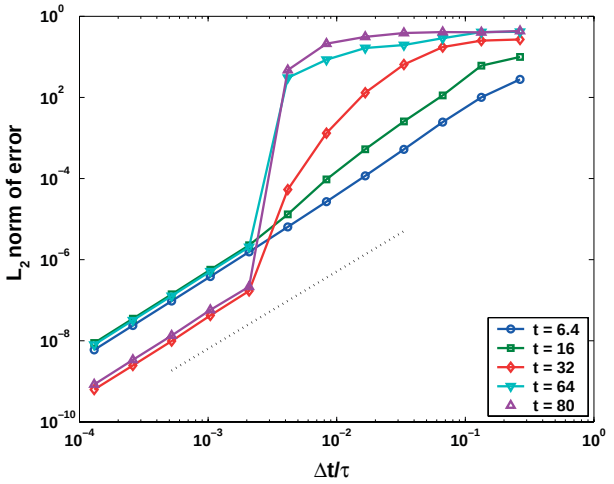

Fig. 10. Brusselator temporal convergence using Romero splitting with $\Delta x = 0.002$. The dotted line is a reference with second-order slope.

with $\Delta t > 0.0125$ steadily grows with time and shows very poor accuracy and no discernible convergence, while the error for runs with $\Delta t < 0.0125$ has very good accuracy and second-order convergence.

In Fig. 11, we show the profile of T at $t = 48$ using FI-2(trap. rule) and Strang DRD, with $\Delta t = 0.2$. In the Strang DRD solution, oscillations are appearing at the boundary. As time progresses these oscillations propagate into the interior of the solution. The period of oscillation τ is 12, so the time step is reasonably below this dynamical time scale. In Fig. 12, we plot the temporal convergence of Strang DRD splitting at $t = 80$ for five different spatial discretizations. Here the reference solution is an extrapolation of solutions using Strang DRD with $\Delta x = 0.0005$. For runs with coarser grids, the time step at which asymptotic second-order convergence is attained is larger than that for runs with finer grids. This is in contrast to the

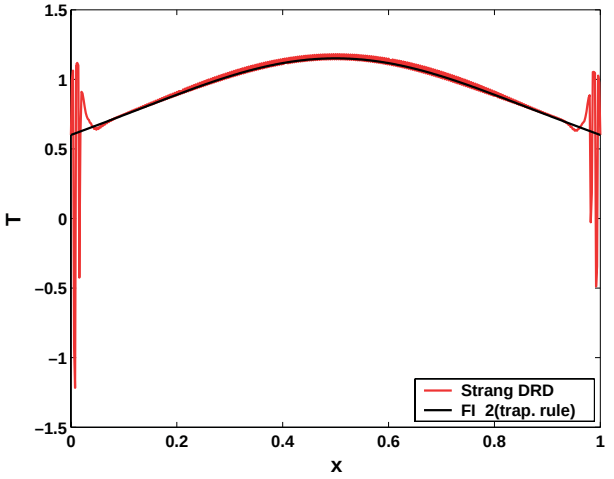

Fig. 11. Brusselator profile at $t = 48$ with $\Delta t = 0.2$.

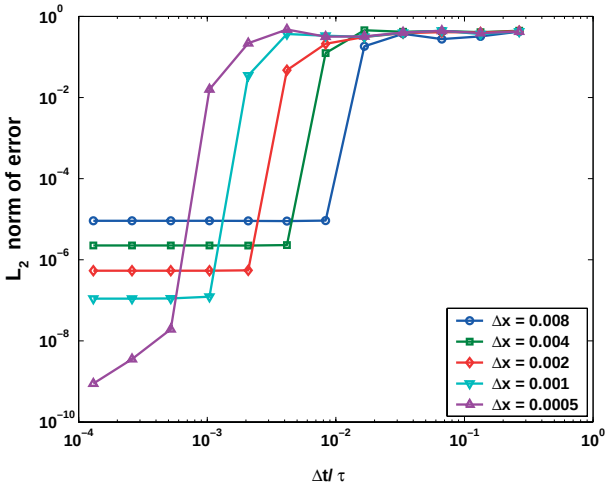

Fig. 12. Brusselator temporal convergence at $t = 80$ using Strang (DRD).

non-split second-order methods that exhibit robust asymptotic convergence for a large region of the temporal time-step parameter range of interest.

This non-convergence of the split methods for reasonable values of Δt is very disturbing. One would expect that, for an oscillation with period τ, a time step somewhat smaller than that required by the Nyquist criteria $\Delta t/\tau = 1/2$ would be sufficient to resolve the dynamical behavior. We often find that $\Delta t/\tau \approx 1/10$ is a useful estimate. For this problem the second-order operator-splitting methods are sampling each period of oscillation with 1000 time steps and still not producing acceptable results. However, the non-split methods show robust convergence, with time steps on the order of the dynamical time scale resulting in significantly more accurate results than the split methods. Even with the pre-asymptotic region of the non-split methods there is at least an order of magnitude difference between the split and non-split methods. Fig. 12 further illustrates this very bad convergence behavior: for a fixed $\Delta t/\tau \approx 10^{-3}$ (i.e., $\Delta t = 0.0125$), if the mesh spacing is refined from $\Delta x = 10^{-3}$ to $\Delta x = 5 \times 10^{-4}$, the L_2 error in the calculation increases by six orders of magnitude. This non-intuitive non-asymptotic behavior is quite unacceptable, and suggests that one needs to exercise caution when using these operator-splitting methods; otherwise the solutions will have an unacceptable error with possibly disastrous consequences.

Preliminary studies to further understand this behavior have been carried out. In our studies it has been observed that this non-intuitive behavior is not due to errors induced in the reaction sub-step calculation. In fact we have seen the counter-intuitive behavior that a less accurate evaluation of the reaction sub-step can actually stabilize the split time integrator. This stabilization then leads to an overall lower L_2 error for a given diffusion step size of $\Delta t/\tau$. These results underscore the fact that these non-balanced operator-splitting schemes can be very sensitive to the effective imbalance introduced by the operator-splitting methods. This conclusion is further supported by the fact that the first-order operator-splitting method, which uses a dissipative integrator for diffusion (backward Euler), is stable while the second-order operator-splitting method using a neutrally stable integrator for diffusion (trapezoidal rule) is unstable. In [7] it is suggested that the reason for the oscillations in the solutions using second-order operator-splitting methods is because the reaction step is too long and the diffusion step is then not able to adequately damp the high-frequency modes. Once the time step is below a critical value, the diffusion step can suitably damp out these modes. Our interpretation of Fig. 12 is that runs on a coarser mesh will have greater artificial dissipation, which then acts to damp out the high frequencies. Thus, for runs using a second-order operator-splitting method

with a relatively large Δt, a solution on a coarse mesh may in fact be more accurate than a solution on a fine mesh. This will be further examined in future work.

As a final note to Fig. 12, the leveling of the L_2 error is due to the spatial error, since the reference solution in this case is the extrapolated solution of the $\Delta x = 0.0005$ solution. It is interesting that, once it reaches the asymptotic regime, the L_2 error drops to the level of the spatial error. This suggests that stability is obtained when the temporal error becomes smaller than the spatial error.

In Fig. 7, for $\Delta t = 3 \times 10^{-3}$, which is within the range where all second-order methods exhibit their asymptotic convergence rate, the range of errors between the most and least accurate methods can vary by one to two orders of magnitude, depending on the time the error is measured. For a fixed error tolerance of 10^{-3}, this corresponds to the required time step ranging by up to an order of magnitude. In this regime the operator-splitting methods are more accurate than FI-2, but FI-2 achieves its rate of convergence at a much larger Δt, and thus is more robust in terms of the time step than the operator-splitting methods. This more robust behavior is very important in the achievement of predictive simulations.

7.3. Blow-up

We selected the times $t = 1.5$ and $t = 2.0$ at which to measure the temporal convergence of the blow-up (LD) and blow-up (ND) solution profiles. At these times the solutions have grown by roughly an order of magnitude. Also, for both problems we chose reference temperatures of $T = 2$ and $T = 100$ at which to study the temporal convergence to the reference times t_2 and t_{100}. These comprise an early time which has a balance between the reaction and diffusion operators and a time near blow-up which is dominated by the reaction operator.

Fig. 13 shows the solution profiles of the blow-up (LD) and blow-up (ND) problems. For both problems the solution initially grows slowly but later grows more rapidly. The blow-up (LD) solution develops a very sharp peak at $x = 0.5$, while the profile of the blow-up (ND) solution stays rather broad even when the solution is large. Also, the blow-up (ND) solution develops nearly infinite derivatives at the boundary, which degrades the spatial convergence.

In Fig. 14, we see that for the blow-up (LD) problem with $\Delta t = 0.0078$, all methods indeed exhibit growth in the solutions at an increasing rate. The second-order methods have very good agreement in

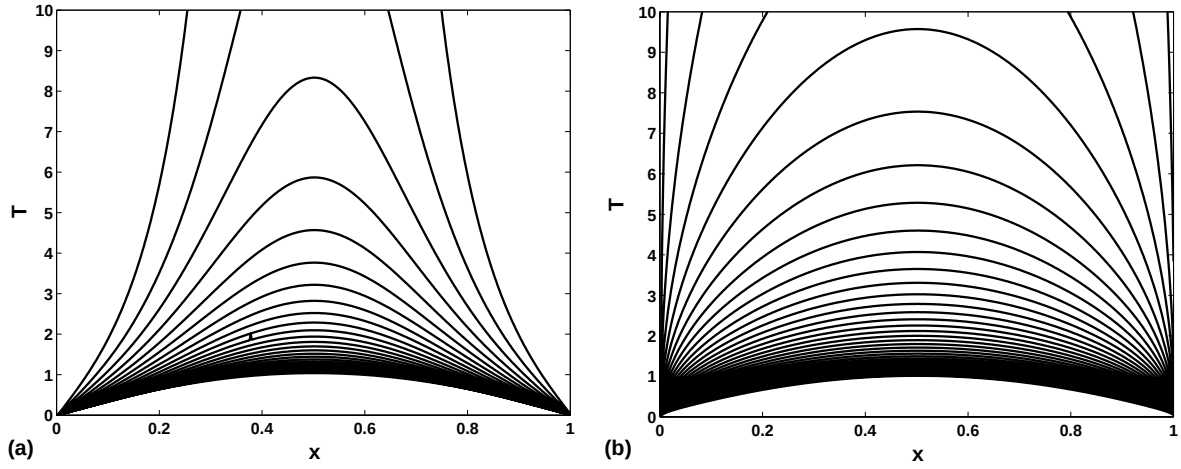

Fig. 13. Blow-up (LD) (a) and blow-up (ND) (b) profiles. Solutions computed using FI-2($\rho_\infty = 0.8$) with $\Delta t = 0.0078$. Profiles plotted at a time interval of 0.0625. Final plot times are (a) 1.5625 and (b) 2.3125.

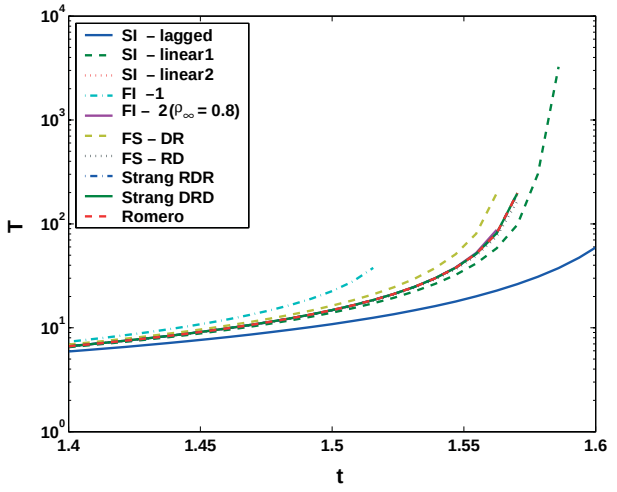

Fig. 14. Blow-up (LD), value of T at $x = 0.5$, $\Delta t = 0.0078$.

values of $T(x = 0.5)$, while the first-order methods differ considerably in both their values of $T(x = 0.5)$ and in their blow-up times.

Fig. 15 shows that the spatial rate of convergence is second order, as expected. The plots in Fig. 16 show that all the methods achieve their asymptotic temporal rates of convergence. For the blow-up (LD) problem, because the second-order split methods are so much more accurate than the fully implicit, an extrapolation of the Romero method was used as the reference solution.

For the SI-lagged, SI-linear 1, and FS-RD, the convergence rate grows slowly and does not reach the asymptotic rate until Δt is quite small, and in fact the SI-lagged method has a rather large non-asymptotic region of convergence. The FS-DR and FI-1 methods have a different problem, in that their solutions reach blow-up before $t = 1.5$ for large Δt. Of the second-order methods, FI-2($\rho_\infty = 0.8$) appears to have the most

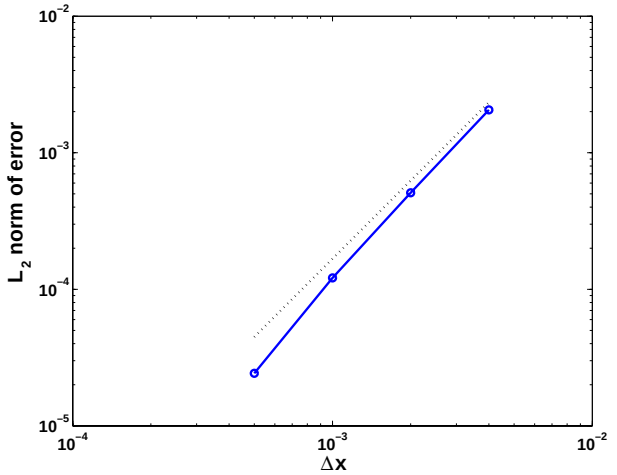

Fig. 15. Blow-up (LD) spatial convergence using Strang RDR with $t = 1.5$ and $\Delta t = 0.002$. Reference solution uses $\Delta x = 0.00025$. The dotted line is a reference with second-order slope.

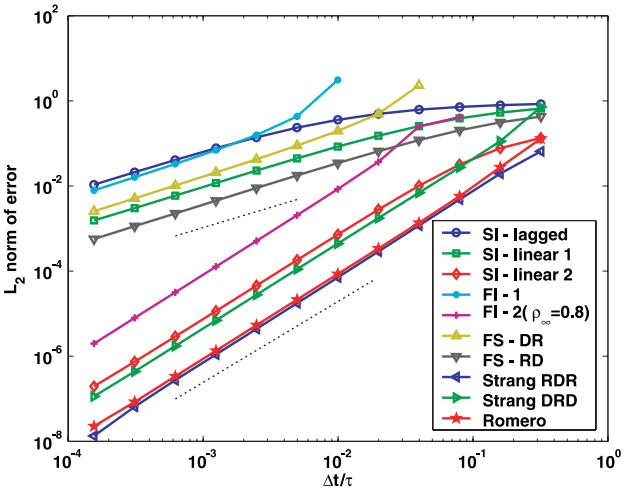

Fig. 16. Blow-up (LD) temporal convergence at $t = 1.5$. The dotted lines are references with first- and second-order slopes.

error. As before, this can be understood in that the operator-splitting methods solve the reaction operator much more accurately, which is the only nonlinear term and is the driving mechanism in this equation.

For a fixed $\Delta t = 10^{-3}$, the error of the first-order methods ranges by two orders of magnitude while the error of the second-order methods ranges by over two orders of magnitude. For that time step the error of the least accurate first-order method is over five orders of magnitude greater than the error of the most accurate second-order method. For an error tolerance of 10^{-2}, the required time steps of the first-order methods range by two orders of magnitude, while, for an error tolerance of 10^{-5}, the required time steps of the second-order methods range by over an order of magnitude. For an error tolerance of 10^{-2} the least accurate first-order method requires a time step almost 1000 times smaller than the time step the most accurate second-order method needs to take.

Fig. 17 shows the temporal convergence to t_2 and t_{100}. For these plots the reference times were computed by Richardson extrapolation of the times computed by the Strang RDR method. The first of these shows

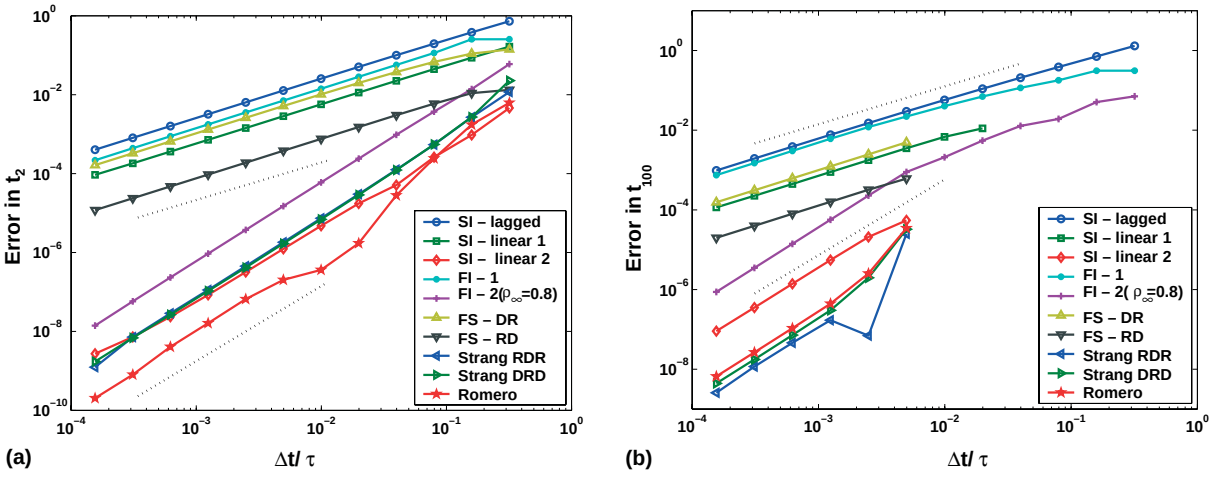

Fig. 17. Blow-up (LD): (a) error in t_2, (b) error in t_{100}. The dotted lines are references with first- and second-order slopes.

the expected convergence rates, although the convergence of the Romero method is somewhat erratic. On the second plot, data for larger time steps of some methods are missing because the numerical solution either blew up or became unphysical before reaching the reference temperature. In the case of the split schemes there was no "recovery" mechanism since the underlying reaction step became unbounded without the balancing diffusion operator. For the fully implicit methods as the nonlinear solution would not converge the time step was reduced so that the method could converge to a solution. Consequently, the errors for larger initial Δt may in fact correspond to a smaller value of effective Δt. This explains the flattening behavior of the convergence plots at the larger Δt for the second order FI methods. However, for smaller Δt this was not necessary and here the expected rates of convergence are achieved.

In each plot the SI-lagged method has the most error of the first-order methods, as expected, while FI-1 has the second most, and FS-DR has the least. Among the second-order methods, FI-2($\rho_\infty = 0.8$) consistently has the most error, but the ordering of the remaining methods varies.

In Fig. 18, we see that the spatial convergence for the blow-up (ND) problem is not second order but is closer to a convergence rate of 1.1. This is because the slope of the solution tends to infinity at the boundaries, thus reducing the rate of convergence. This behavior would be consistent with an order reduction due to nearly discontinuous behavior at the end points of the domain.

Fig. 19 shows the temporal convergence to the solution of the blow-up (ND) problem at the time $t = 2$, while Fig. 21 shows the temporal convergence to t_2 and t_{100}. One interesting difference from the blow-up (LD) problem is that the accuracy FI-2($\rho_\infty = 0.8$), both in terms of the relative L_2 error and in terms of the error in t_2 and t_{100}, is better than that of either of the Strang splittings for most values of Δt. This is also true in Fig. 20, which shows the convergence of the second-order methods at $t = 0.5$. At this early time the FI-2($\rho_\infty = 0.8$) method is the most accurate of the second-order methods.

The reason for this change in relative accuracy of the different methods on the convergence is likely because the nonlinearity in the diffusion makes that term more significant than it was in the blow-up (LD) problem. The diffusion and reaction terms are more balanced in magnitude, thus making the error due to splitting the operators more significant. This is also seen in Fig. 21, where at the earlier time t_2, when the reaction and diffusion terms are more balanced, the FI-2 method is more accurate than the operator-splitting methods. At t_{100}, though, when the solution is closer to blow-up and the reaction term is larger, the

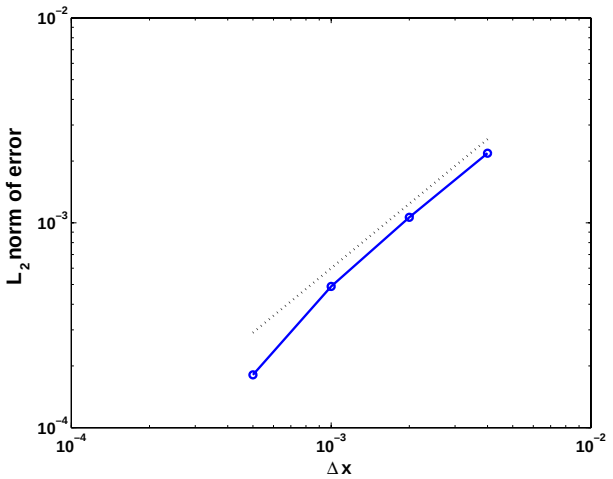

Fig. 18. Blow-up (ND) spatial convergence using Strang RDR with $t = 2$ and $\Delta t = 0.002$. Reference solution uses $\Delta x = 0.00025$. The dotted line is a reference with slope of 1.1.

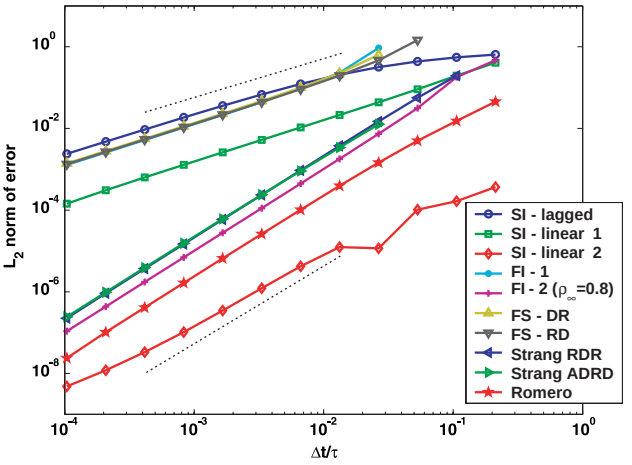

Fig. 19. Blow-up (ND) temporal convergence at $t = 2.0$. The dotted lines are references with first- and second-order slopes.

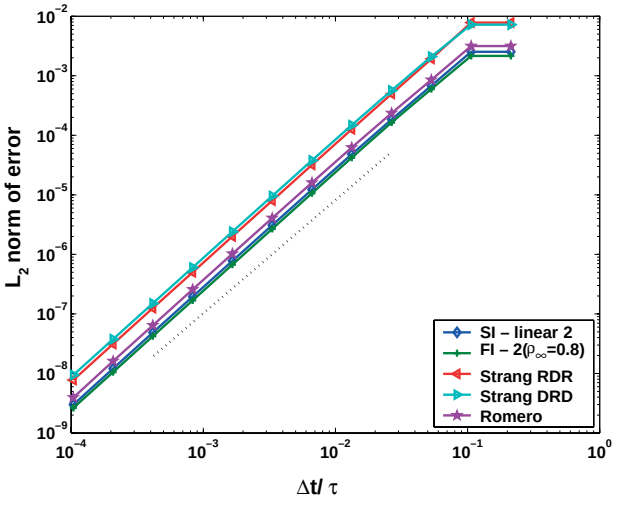

Fig. 20. Blow-up (ND) problem, temporal convergence of second-order methods, $t = 0.5$. The dotted line has a reference slope of 2.

FI-2 method has comparable accuracy as the Strang DRD method and is less accurate than Romero splitting.

Another interesting observation is that the SI-linear 2 has very good accuracy for this problem. It is the most accurate method at $t = 2$, and its t_2 error is an order of magnitude less than that of the next most accurate method, while its t_{100} error is lowest by two orders of magnitude. This is surprising, because SI-linear 2 does not converge the nonlinearities, while the FI-2 methods do. However, in [14] Lowrie shows that for some problems SI-linear 2 has better accuracy than FI-2 methods.

For $\Delta t = 10^{-3}$ the errors for the first-order methods range by over an order of magnitude while the errors of the second-order methods range by over two orders of magnitude. For that time step the error of the least accurate first-order method is nearly six orders of magnitude greater than that of the most accurate

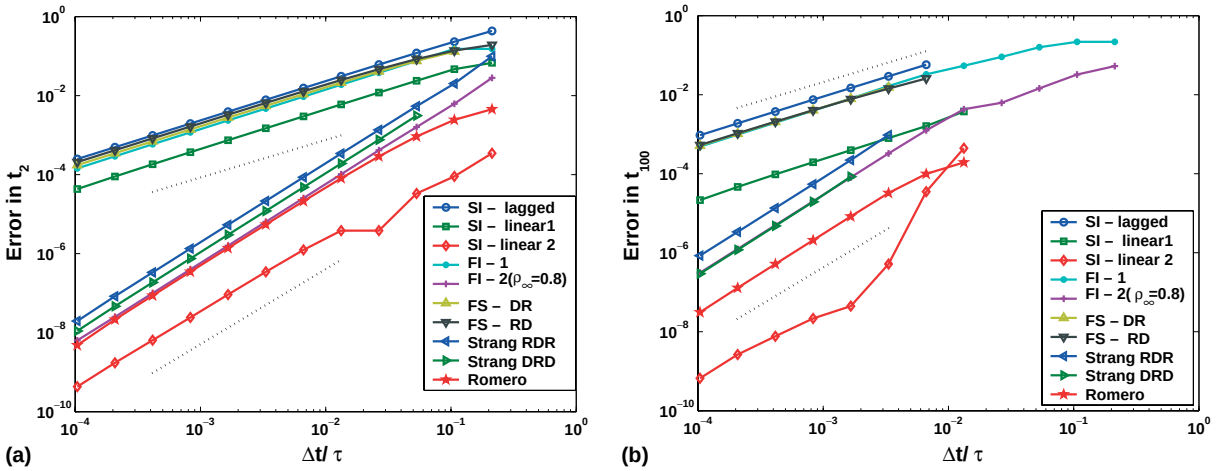

Fig. 21. Blow-up (ND): (a) error in t_2, (b) error in t_{100}. The dotted lines are references with first- and second-order slopes.

second-order method. For an error tolerance of 10^{-2} the required time step for the first-order methods ranges by over an order of magnitude, as does the required time step for the second-order methods for an error tolerance of 10^{-6}.

7.4. Non-equilibrium radiation diffusion

Profiles of the solution of the radiation–diffusion problem are shown in Fig. 22. For both T and E the solution is a front propagating to the right, with a discontinuous derivative at the front. As with the boundary in the blow-up (ND) problem, this sharp front is difficult to resolve on a fixed grid, and we expect the spatial convergence to degrade.

Fig. 23 shows the spatial convergence for the radiation–diffusion problem using the FI-2(trap. rule) method with lumped mass and source. The plot is somewhat erratic and the convergence appears to be less

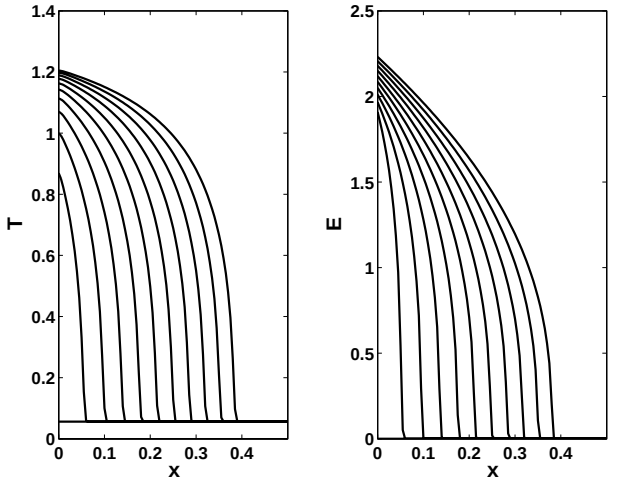

Fig. 22. Radiation-diffusion profile. Solutions computed using Strang RDR and are plotted at a time interval of 0.1.

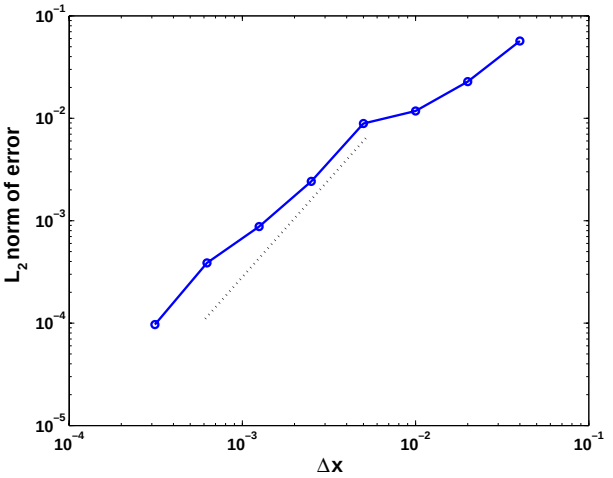

Fig. 23. Radiation-diffusion spatial convergence using FI-2(trap. rule) with $t = 1$ and $\Delta t = 0.0003125$ with $\Delta x = 0.005$. Reference solution is FI-2 (lumped mass and source) for the reference solution. The dotted lined is a reference with second-order slope.

than second order. As mentioned above, this is not surprising because the solution has a discontinuity in the derivative at the leading edge of the front.

For all methods, both the mass and the source terms were lumped in order to control oscillations at the leading edge of the front. The SI-lagged and SI-linear 2 method was unstable for large values of Δt, so only the data for those runs that converged are presented here. Regarding the SI-linear 2 method, unlike the other test cases the source term in this problem is too complex for its Jacobian to be expressed analytically. Therefore, the Jacobian was computed numerically.

The temporal convergence of the methods is presented in Fig. 24. This figure summarizes the temporal accuracy behavior for the various methods and uses a reference solution based on an extrapolation

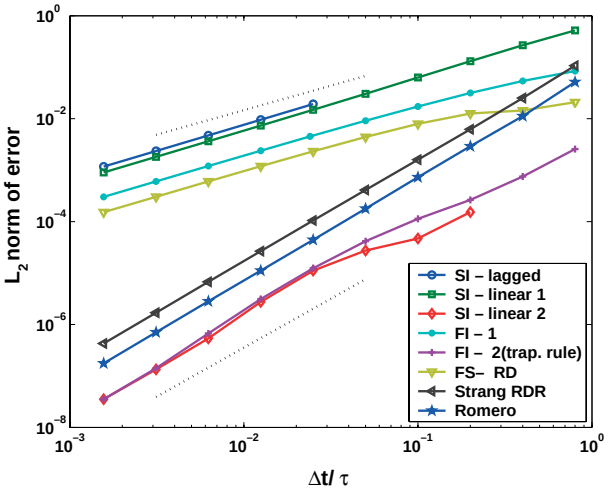

Fig. 24. Radiation-diffusion temporal convergence with $\Delta x = 0.005$ and using FI-2 (lumped mass and source) for the reference solution. The dotted lines are references with first- and second-order slopes.

of solutions using the FI-2(trap. rule) method. All the methods exhibit their expected asymptotic order of convergence. For this problem the FI-2 method appears to have better accuracy than either the Strang RDR or the Romero splitting methods. In this case the SI-linear 2 and the FI-2(trap. rule) methods have very similar relative error characteristics. Of the first-order methods, the FI-1 method has less error than the SI-lagged and SI-linear 1 methods, but has more error than the first-order operator-splitting method.

The range of error for a fixed Δt is an order of magnitude for the first-order methods and as much as two orders of magnitude for the second-order methods between the operator-splitting and FI methods. These correspond to a range of Δt for a fixed error of an order of magnitude for both the first-order methods and second-order methods. For $\Delta t = 4 \times 10^{-5}$ the variation in error for the least accurate first-order methods and the most accurate second-order methods is over four orders of magnitude. In terms of robustness the SI-lagged method fails to converge for larger time step sizes as does the SI-linear 2 method. A more extensive discussion on the details of the radiation–diffusion problem and the performance of the various time integration methods can be found in [18].

8. Conclusions

In this paper, we have studied the accuracy and rates of convergence of time integration methods applied to a suite of nonlinear reaction–diffusion test problems. These different test cases model a variety of behavior, including front propagation, oscillations, and blow-up. With these test cases we have presented: spatial convergence studies to verify the expected order of accuracy of the FE method; specific implementations of the semi-implicit lagged and linearized methods along with operator-splitting techniques and fully implicit methods; and the temporal accuracy for each method.

Our results have demonstrated that in general each of the time integration methods will exhibit its asymptotic rate of temporal convergence for each of the problems. There are notable exceptions, however. As is demonstrated in the blow-up problem, the lagged method can have slow convergence for large values of the time step. In the case of the Brusselator problem it was demonstrated that the asymptotic region of convergence may only be obtained for unacceptably small times step sizes for the second-order operator-splitting methods. This example problem, with reaction and diffusion operators that are nearly balanced, points out a number of very disturbing issues associated with the non-balanced operator-splitting methods. The temporal non-convergence region for the operator-splitting methods was demonstrated to be much larger than that for the fully implicit methods. In addition the counter-intuitive behavior of the sequence of temporal refinement studies for various levels of spatial refinement was equally disturbing.

While it is not possible to draw consistent general conclusions about the accuracy of all the methods, it is possible to make some observations. The semi-implicit lagged method appears to often be the least accurate of the first-order methods. This is perhaps not surprising, because it uses less information from the new time step than any other method. It also appears that the operator-splitting methods have somewhat of a "split personality". Specifically, on a subset of the test problems (thermal wave and blow-up (LD)) these methods are the most accurate. This increased accuracy is most likely due to the low error tolerances on the reaction sub-step solves compensating the increased error due to the operator-splitting procedure. However, the stability and accuracy results for the operator-splitting methods on the more difficult test problems (Brusselator, blow-up (ND), and radiation–diffusion) are much less favorable. Clearly the results from the Brusselator problem demonstrate the possible significant impact on stability and accuracy of the non-balanced operator-splitting methods. In general, while the fully implicit methods are not always the most accurate techniques, this was often the case for the difficult coupled systems of nonlinear equations. In addition these methods appear to have a more robust (regular) convergence behavior for larger time steps, which is important for complex multiple time scale simulations.

References

[1] C. Bandle, H. Brunner, Blowup in diffusion equation: a survey, Journal of Computational and Applied Mathematics 97 (1998) 3–22.
[2] R.L. Bowers, J.R. Wilson (Eds.), Numerical Modeling in Applied Physics and Astrophysics, Jones and Bartlett, Boston, 1991.
[3] J. Brackbill, B. Cohen (Eds.), Multiple Time Scales, Academic Press, Orlando, 1985.
[4] P.N. Brown, C.S. Woodward, Preconditioning strategies or fully implicit radiation diffusion with material-energy transfer, SIAM Journal of Scientific Computing 23 (2) (2001) 499–516.
[5] J. Chung, G.M. Hulbert, A time integration algorithm for structural dynamics with improved numerical dissipation: the generalized-α method, Journal of Applied Mechanics 60 (1993) 371–375.
[6] S.D. Cohen, A.C. Hindmarsh, CVODE, a stiff/nonstiff ODE solver in C, Computers in Physics 10 (2) (1996) 138–143.
[7] D.J. Estep, S. Tavener, Notes on determining stability of split-step integrators using green's functions, personal communication.
[8] C.A.J. Fletcher, Computational Techniques for Fluid Dynamics, vol. 1, Springer, Berlin, 1988.
[9] K.E. Jansen, C.H. Whiting, G.M. Hulbert, A generalized-α method for integrating the filtered Navier–Stokes equations with a stabilized finite element method, Computer Methods in Applied Mechanics and Engineering 190 (2000) 305–319.
[10] O.M. Knio, H.N. Najm, P.S. Wyckoff, A semi-implicit numerical scheme of reacting flow: II. Stiff, operator-split formulation, Journal Computational Physics 154 (1999) 428–467.
[11] D.A. Knoll, L. Chacon, L.G. Margolin, V.A. Mousseau, On balanced approximations for time integration of multiple time scale systems, Journal of Computational Physics 185 (2003) 583–611.
[12] D.A. Knoll, W.J. Rider, G.L. Olson, An efficient nonlinear solution methods for non-equilibrium radiation diffusion, Journal of Quantitative Spectroscopy and Radiative Transfer 63 (1999) 15–29.
[13] D.A. Knoll, W.J. Rider, G.L. Olson, Nonlinear convergence, accuracy and time step control in non-equilibrium radiation diffusion, Journal of Quantitative Spectroscopy and Radiative Transfer 65 (2001) 25–36.
[14] R.B. Lowrie, A comparison of time integration methods for nonlinear relaxation and diffusion, Journal of Computational Physics (accepted for publication).
[15] G.I. Marchuk, On the theory of the splitting-up method, in: Proceedings of the 2nd Symposium on Numerical Solution of Partial Differential Equations, SVNSPADE, 1970, pp. 469–500.
[16] V.A. Mousseau, D.A. Knoll, W.J. Rider, Physics-based preconditioning and the Newton–Krylov method for non-equilibrium radiation diffusion, Journal of Computational Physics 160 (2000) 743–765.
[17] Y.Y. Nie, V. Thomee, A lumped mass finite element method with quadrature for a non-linear parabolic problem, IMA Journal of Numerical Analysis 5 (1985) 371–396.
[18] C.C. Ober, J.N. Shadid, Studies on the accuracy of time-integration schemes for the radiation–diffusion equations, Journal of Computational Physics (2004), in press.
[19] E.S. Oran, J.P. Boris, Numerical Simulation of Reactive Flow, Cambridge University Press, Cambridge, 2001.
[20] I. Prigogine, R. Lefever, Symmetry breaking instabilities in dissipative systems, ii, Journal of Chemical Physics 48 (4) (1968) 1695–1700.
[21] L.A. Romero, On the accuracy of operator-splitting methods for problems with multiple time scales, Technical Report SAND2002-1448, Sandia National Laboratories, August 2002.
[22] C. J. Roy, Grid convergence error analysis for mixed-order numerical schemes, AIAA Paper 2001-2606, 2001.
[23] A.A. Samarskii, V.A. Galaktionov, S.P. Kurdyumov, A.P. Mikhailov, Blow-up in Quasilinear Parabolic Equations, de Gruyter Expositions in Mathematics, vol. 19, Walter de Gruyter, Inc, Berlin, 1995.
[24] J.N. Shadid, A.G. Salinger, R.C. Schmidt, T.M. Smith, S.A. Hutchinson, G.L. Hennigan, K.D. Devine, H.K. Moffat, A finite element computer program for reacting flow problems, Part 1: theoretical development, Technical Report SAND98-2864, Sandia National Laboratories, January 1999.
[25] L.F. Shampine, M.W. Reichelt, The matlab ode suite, SIAM Journal of Scientific Computing 18 (1) (1997) 1–22.
[26] B. Sportisee, An analysis of operator splitting techniques in the stiff case, Journal of Computational Physics 161 (2000) 140–168.
[27] G. Strang, On the construction and comparison of difference schemes, SIAM Journal of Numerical Analysis 5 (3) (1968) 506–517.
[28] R.H. Szilard, G.C. Pomraning, Numerical transport and diffusion methods in radiative transfer, Nuclear Science and Engineering 112 (1992) 256–269.
[29] V. Thomée, Galerkin Finite Element Methods for Parabolic Problems, Springer-Verlag, New York, 1997.
[30] N.N. Yanenko, The Method of Fractional Steps, Springer-Verlag, New York, 1971, Translation Ed. M. Holt.